Structure-Function Relationship of the Na^+ Glucose Cotransporter SGLT1: Interaction of Loop 13 with Various Inhibitors and Lipid Membranes

Dissertation
Submitted to the Department of Biophysical Chemistry
of the University of Dortmund, Germany
for the Degree of *Doctor Rerum Naturalium*

Completed at
Max Planck Institute of Molecular Physiology, Dortmund, Germany

By
Mobeen Raja
(Masters of Science in Biochemistry)

Dortmund, 2004

The research work described in this thesis was carried out in the period from January 2002 to September 2004 at the Max Planck Institute of Molecular Physiology, Dortmund, Germany, under the supervision of Prof. Dr. Dr. h.c. Rolf K.H. Kinne in the Department of Epithelial Cell Physiology.

I am grateful to Prof. Dr. Dr. h.c. **Rolf K.H. Kinne** for choosing such an interesting combination of Molecular Biology and Biophysical Chemistry for my Ph.D studies, as well as his sympathetic and moral support to carry out my work in a successful manner.

1. Referee: Prof. Dr. Dr. h.c. Rolf K.H. Kinne
2. Referee: Prof. Dr. Roland Winter

To My Parents

and

Sincere Friends

Acknowledgements

I deem it a great privilege to gather all my emotions and sentiments to express deep sense of veneration to my soul supervisor Prof. Dr. Dr. h.c. Rolf K.H. Kinne, Department of Epithelial Cell Physiology, Max Planck Institute of Molecular Physiology, Dortmund, for his inexhaustible encouragement, extraordinary patience, and praise worthy attitude on carrying out my research work and accomplishing this thesis.

I would like to pay my sincere regards to Prof. Dr. Roland Winter, Department of Physical Chemistry I, University of Dortmund, as my thesis advisor for his invaluable discussions and suggestions for my research project.

I am also thankful to my lab colleagues Xia Xiaobing and Navneet Tyagi for their experimental help and healthy discussions to sacrifice my projects successfully. I pay my special thanks to Dr. Helmut Kipp for providing me with a photoactive compound for photolabeling studies.

I owe a lot of thanks to Dr. Peter Hinterdorfer, Barbara Wimmer and Miss Aom from the Department of Biophysics, University of Linz, Linz Austria, as our research collaboratives, for their wonderful appreciations regarding my research work and furthermore allowing me to strengthen the scientific as well as friendly connections.

It was my great pleasure to work with my lab members, Kirsten Michel, Hendrike Schuetz and Jutta Luig who contributed a lot to my research work by getting a proper guidance to learn many lab techniques. I am highly indebted to them for such a great experience.

Many thanks are due to my dear and sweet friends especially Daniel Scharlau, Frank ter Veld, Heidrun Olsen, Jonathan Müller, Nadeem Javid, Supriya Subramaninan and Thorsten Althoff for helping me professionally, as well as emotionally in the course of hard times throughout my stay.

I would like to pay my gratitude to all of my IMPRS colleagues for sharing a nice and active atmosphere with me.

I am very thankful to the International Max Planck Research School in Chemical Biology (IMPRS-CB) for funding the present research work. The contributions of Prof. Dr. Dr. Rolf K.H. Kinne as a spokesperson and Dr. Jutta Roetter as a graduate school coordinator are gratefully acknowledged for organizing laboratory rotations, practical courses, lecture series, retreats and scientific meetings which helped me a lot to increase my knowledge and to serve in the scientific community.

My special thanks are due to Stefan Adamsmair for his moral support which helped me extensively to achieve a certain level of patience in completing my work.

At the end, I have no words to pay my cordially thanks to my loveable parents, brother and sisters for their encouragements and appreciations in carrying out my studies successfully.

Contents

1. INTRODUCTION

1.1. Sodium-D-Glucose Cotransporter SGLT1

The life of every organism depends on the continuous supply of energy. One of the most important metabolic fuels is D-glucose. In mammals, glucose transport is mediated by a number of integral membrane proteins known as specific carriers. They are involved in the absorption of glucose through the proximal tubular segment of the nephron and intestinal epithelial cells. The glucose is returned to the circulation to maintain its blood levels and to provide other cells with a source of energy for various metabolic requirements (Hirayama *et al*., 1997; Loo *et al*., 1998). At present about five facilitated-diffusion glucose transporters (GLUT-1 to GLUT-4 and GLUT-7) are believed to exist in mammalian cells. In addition, sodium glucose cotransporters (SGLTs) are known to be involved in glucose uptake (Loo *et al*., 1998; Vayro *et al*., 1998). Members of the sodium/glucose cotransporter family are found throughout the living organisms as they transport a wide variety of substrates (sugars, inositol, iodide, urea and proline) into the cell using the electrochemical gradient of cations like Na^+, Li^+, or H^+ (Veenstra *et al*., 2002; Michael *et al*., 2000; Turk & Wright, 1997; Wright *et al*., 1998; Wright, 2001). For example, the extent of Na^+ - dependent glucose absorption is dependent upon SGLT1 protein content (Fringes *et al*., 2001; Murer *et al*., 1974; Beck and Sacktor, 1975). The SGLT1 is a high-affinity glucose transporter (*K*m ~100 μM; Wright, 1993) that couples glucose transport into the cell to an inwardly directed Na^+ gradient (Figure 1.1). This Na^+ gradient is maintained by Na^+/K^+-ATPase in the basolateral membrane. The stoichiometry of the process dictates that two Na^+ cross the membrane with each glucose molecule. SGLT1 has been demonstrated to transport in addition 210 water molecules along with each glucose (Meinild *et al*., 1998).

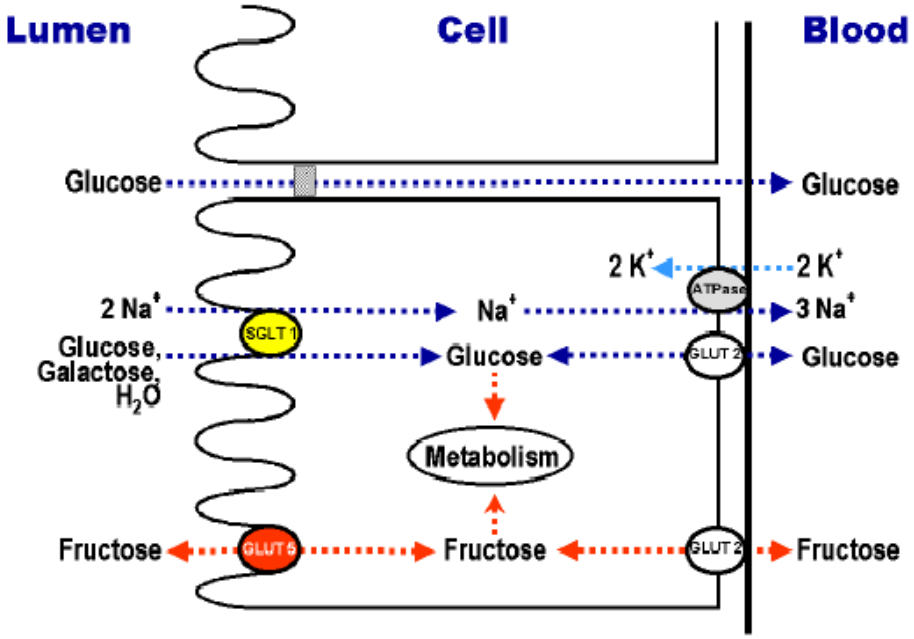

FIG. 1.1. Glucose transport in enterocytes. The Na^+-dependent glucose transporter (SGLT1) is located in the apical membrane and transports Na^+ (two) coupled with glucose or galactose and water. This transport is driven by the inwardly directed Na^+ gradient, which is maintained by the activity of Na^+/K^+-ATPase in the basolateral membrane. The facilitative transporter GLUT2 transports sugars across the basolateral membrane, whereas the facilitative transporter GLUT5 transports fructose across the apical membrane (adapted from Wright, 1993).

Coupling of glucose, sodium flux and translocation of the compounds are supposed to be accompanied by conformational changes of the protein. Such changes could be induced for example by Na^+, which increases the cotransporter's affinity for sugar (Panayotova *et al*., 1997; Lo and Silverman, 1998). Mutagenesis studies revealed that the N-terminal half of the peptide contains the Na^+ binding sites, as amino acids 162-173 apparently constitute a part of an external Na^+ pore in the SGLT1 peptide, while glucose binds and permeates through the C-terminal half of the cotransporter since Gln 457 and Thr 460 control sugar-binding (Diez-Sampedro *et al*., 2001; Diedrich, 1966; Oulianova *et al*., 2001; Oulianova and Berteloot, 1996). It is believed that the substrate recognition and translocation by a transporter is a multi step process. Therefore, determination of interaction sites between the sugar and the protein is an important step in elucidating the structural factors that determine specificity in the sugar-binding site and allow studies on characterization of the translocation pathway.

1.2. Transport Inhibitors of Sodium-D-Glucose Cotransporter SGLT1

Inhibition of glucose uptake in the small intestine is a helpful way for reducing the blood glucose level in diabetic patients. SGLT1 has been identified as a potential target in the treatment of diabetes, and inhibitors of the transporter are therefore of renewed interest (Hirayama *et al*., 2001; Diedrich, 1966). The cotransport system is inhibited by glucosides with either aromatic or aliphatic aglucone residues. Phlorizin, a β-glucoside of the aromatic compound phloretin (Figure 1.2), is the most potent competitive inhibitor, with an apparent K_i value of 1 μM (Oulianova and Berteloot, 1996; Hirayama *et al*., 2001). Phloretin, the aglucone of phlorizin (Figure 1.2), is produced by hydrolysis of phlorizin (Hunter, 1993) by removing the glucose moiety of phlorizin. Phloretin has a strong inhibitory effect on sugar uptake by SGLT1 (Panayotova *et al*., 1997). Both agents are found in apple tree foliage. The conformation of phlorizin exhibits an extended coplanar arrangement of the two aromatic rings A and B (Figure 1.2). Phlorizin consists of a pyranoside ring and two aromatic rings joined by an alkyl spacer. According to the studies performed by Wielert Badt *et al*., 2000, hydrogen bonds from the 2-, 3-, 4-, and 6-OH groups of the pyranoside ring and from the 4′- and 6′-OH groups of the aromatic ring A, and hydrophobic elements in the same two structures are involved in phlorizin binding to SGLT1.

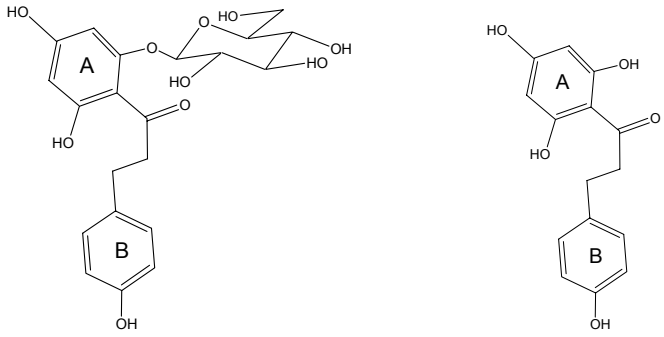

I **II**

FIG. 1.2. Chemical structure of Phlorizin and phloretin. **I: Phlorizin,** The molecule is subdivided into three segments: pyranoside ring, aromatic ring A, and aromatic ring B. **II: Chemical structure of an aglucone of phlorizin, phloretin [3-(4-hydroxyphenyl)-1-(2,4,6-trihydroxyphenyl)-1-propanone].**

It is proposed that phlorizin binding to SGLT1 is a two-step process: rapid formation of an initial collision complex followed by a slow isomerization process that occludes phlorizin within its receptor site (Oulianova *et al*., 2001). Phlorizin is thereby supposed to bind to both the sugar binding site and the aglucone binding site, the latter with a hydrophobic/aromatic surface (Oulianova and Berteloot, 1996; Hirayama *et al*., 2001). Site-directed mutagenesis studies suggest that a hydrophobic region, located in the c-terminus of SGLT1 (amino acids 604-610), is critically involved in the binding of phlorizin (Novakova *et al*., 2001).

Beside phlorizin, which exhibits an aglucone moiety of a rather complicated structure, alkyl glucosides, also, have been demonstrated to inhibit sodium-D-glucose cotransport in rabbit, elasmobranch, rat and human brush border membrane vesicles (Kipp *et al*., 1996 and 1997). Alkyl glucosides differ in size depending upon the alkyl side chain length. Increase in length of the side chain from 6 to 9 carbon atoms leads to a maximum inhibition, whereas very short and very long side chains cause only moderate inhibition of SGLT1. Moreover, in skate and shark BBMV, *n*-alkyl-*β*-D-glucosides are significantly more effective inhibitors than the corresponding *α*-anomers (Kipp *et al*., 1997).

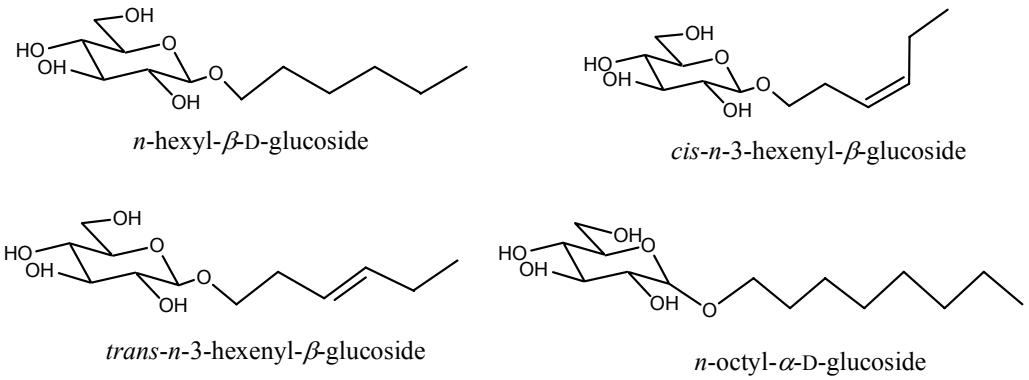

FIG 1.3. Chemical structures of alkyl glucosides and unsaturated *n*-hexenyl analogs used in this study.

In addition, a flexible side chain is required for maximal inhibition as the unsaturated compound *cis*-*n*-hexenyl-*β*-glucoside is a significantly more effective inhibitor than the corresponding *trans*-isomer (Figure 1.3). This indicates that for an optimum

simultaneous interaction with the D-glucose binding site and hydrophobic domains of the transporter, *n*-alkyl-*β*-D-glucoside has to exhibit a coiled conformation (Kipp *et al*., 1996).

1.3. Topology of Sodium-D-Glucose Cotransporter SGLT1

The intestinal Na^+/glucose cotransporter SGLT1 was expression-cloned in 1987, and found to be the first member of a new gene family. Information on the orientation of SGLT1 within the membrane can provide essential clues in understanding the structure/function relationship of this important cotransporter protein. To establish a topology for a membrane protein, strategies combining computer calculation, modeling and experimental tests are usually employed. The initial steps include use of the hydropathy analysis (Kyte and Doolittle, 1982), the multiple sequence alignment algorithm (Vingron and Agros, 1988), and the approximation of the loop's orientation using the positive-inside rule of von Heijne (1992). A secondary structure model of SGLT1 proposed by Turk *et al*., 1996, is shown in Figure 1.4. The protein consists of 662-665 amino acid residues with 14 putative transmembrane domains joined through several extracellular or intracellular loops (Turk and Wright, 1997). Experimental and computational analyses indicate that all transmembrane spans are presumably alpha-helical (Engelman and Steitz, 1981; Jacobs and White, 1989). An important contribution for clarification of the structure and function relationship of the transporter would be if topology of the extramembranous loops that flank the membrane spans could be clearly assigned.

The topology of SGLT1 within the membrane is still a matter of argument. The localization of the loop residues, particularly the large loop close to the C-terminal end (amino acid residues 541-638) which links the transmembrane helices 13 and 14 (in short, loop 13) has been placed either facing the cytosol or the extracellular space as examined by several authors using different experimental approaches (Table 1.1).

Table 1.1. Comparison of Topology of Loop 13 Using Different Prediction Methods

Amino acid residues	His-tag or wild type (Lin *et al*., 1999)	Exon correlation (Turk *et al*., 1994)	Glycosylation scan (Turk *et al*., 1996)
584-589	Extracellular	Extracellular	Intracellular
606-630	Extracellular	Extracellular	Intracellular
622-627	Extracellular	Extracellular	Intracellular
662 +	Intracellular	Intracellular	Extracellular

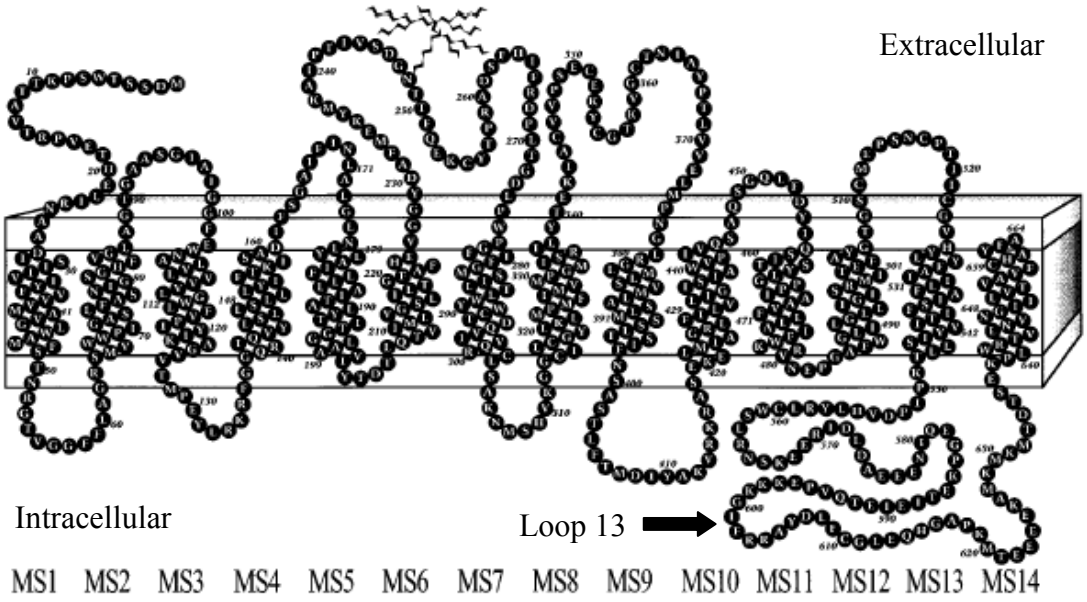

Figure 1.4. A secondary structure model of SGLT1 provided by Turk *et al.* (1996). The topology reveals 14 transmembrane regions, 13 intracellular and extracellular loops. In this model, the location of loop 13 was shown as intracellular.

The determination of topology by an appropriate method is still required to assign which parts of the transporter form intracellular and extracellular regions in order to understand the role of various parts of the transporter during translocation and inhibitor complex formation.

1.4. Use of Domains to Study the Structure-Function Relationship

Eukaryotic membrane proteins are particularly difficult to work with. The expression of small peptides as functional domains of the transporters can be favoured by using suitable hosts. Domains are known as the regions along a single polypeptide chain that can act as independent units. To that extent, they can be excised from the chain, and still be shown to fold correctly, and often still exhibit biological activity (Sierra *et al*., 2000; Kachalsky *et al*., 1995). The regions between domains will also tend to be fairly simple at a sequence level, often being rich in one or two specific amino acids. This would be particularly useful for membrane proteins in which the function of the cytoplasmic or extracellular domain is not clear (Lockwood *et al*., 2003; Selinksky, 2003). Since loop 13 is involved in interaction of an inhibitor, phlorizin, the *in vitro* expression of this domain can provide direct information of the role of various parts

of the peptide during substrate coupling and inhibitor complex formation when the whole transporter is not available.

2. THE AIMS

Over the last 30 years, studies using intact membrane vesicles have greatly contributed to the characterization of Na^+-dependent D-glucose cotransport (SGLT) in terms of substrate and inhibitor specificities. In order to examine the involvement of different parts of the transporter in interaction with various substrates and inhibitors, it is of great interest to understand the mechanism of sequence specific interaction.

Our previous site-directed mutagenesis experiments on the glucose transporter performed in intact vesicles on a full length protein indicated that C-terminal loop 13 is involved in phlorizin binding (Novakova *et al*., 2001). The aim of the present study was to confirm this part of SGLT1 as a phlorizin binding domain and to understand the mechanism of interaction in more detail. We sought to work on this approach by over-expressing mutant loop 13 as a functional domain *in vitro* that carried single tryptophans at different positions as reporter molecules. We wanted to know whether the affinity of phlorizin as a potent inhibitor of SGLT1 in the intact carrier is comparable to the affinity in an isolated system, to determine the sites of interaction in the putative binding pocket, and follow the conformational changes occurring in different regions of the peptide when phlorizin interacts with loop 13. As another goal of the study, we wanted to forward the same experimental approach to determine whether loop 13 also interacts with another type of glucose cotransport inhibitors, called alkyl glucosides (Kipp *et al*., 1996) and whether we can observe the conformational changes in the peptide to compare the differences between the mode of interaction of phlorizin and/or alkyl glucoside with loop 13.

Another purpose of the study was to determine the topology of loop 13 in the membrane which is still under a dim light. The previous approaches applied to determine the topology could not assign the exact orientation of this part of the SGLT1 either inside or outside the membrane. In the forefront to this aim, the point of interest was to determine the small sequences of the peptide which can interact with the membrane and induce conformational changes upon such interactions. To establish a well-defined reconstitution system of loop 13 and lipid vesicles, the knowledge of different composition of lipids was required to understand the mode of lipid-peptide interaction. Furthermore, the reconstitution studies were aimed to get information about the depth of penetration of loop 13 into the lipid membrane.

3. EXPERIMENTAL PROCEDURES

3.1. Materials

Taq DNA polymerase, T4 DNA ligase, restriction enzymes, pCR 2.1-TOPO cloning vector, and dNTP's were obtained from Promega (Mannheim, Germany), New England Biolabs (Schwalbach, Germany) or Invitrogen (Karlsruhe, Germany). Oligonucleotides were synthesized by MWG Biotech (Ebersberg, Germany). pGEX-4T-1 vector and BL21 (DE3) cells were from Novagen (Madison, WI) respectively. Lysozyme, and protease inhibitor cocktail were purchased from Sigma (Taufkirchen, Germany) or Roche Biochemicals (Mannheim, Germany). Thrombin was purchased from Sigma. Dioleoylphosphatidylcholine (DOPC), synthetic 1-Palmitoyl-2-stearoyl (*n*-doxyl)-*sn*-glycero-3-phosphocholine (doxyl PC), with the spin labels at the 5- and 12-positions of the *sn*-2-acyl chain, and dioleoylphosphatidylglycerol (DOPG) were purchased from Avanti Polar Lipids Inc. The following chemical reagents were from Gerbu Biotechnik (Gailberg, Germany), Sigma or Roth (Karlsruhe, Germany) available in the highest purity: EDTA, Tris-base, glycine, NaCl, L-Trp, phlorizin, phloretin, *n*-hexyl-β-D-glucoside, *trans*-*n*-3-hexenyl-β-D-glucoside, *cis*-*n*-3-hexenyl-β-D-glucoside, *n*-octyl-β-D-glucoside, *n*-decyl-β-D-glucoside, 1-hexanol, isopropyl-β-D-thiogalactopyranoside, 2,5-dihydroxybenzoic acid (DHB) and α-cyano-4-hydroxycinnamic acid (CHCA).

3.2. Molecular Biology

A coding sequence was amplified by a standard Polymerase Chain Reaction (PCR) and the product was purified using the normal primers flanking the mutation site to produce an insert with *BamH*I and *Eco*RI restriction sites. The resulting 222-base pair fragment was isolated from 1.5% agarose gel and ligated in to pCR 2.1-TOPO cloning vector and sequenced prior to mutagenesis.

3.3. Site-Directed Mutagenesis

Mutagenesis experiments were performed using Chameleon Double Stranded, Site-directed Mutagenesis Kit (Stratagene, CA) according to the manufacturer's instructions. The following oligonucleotides with mutated nucleotides (underlined) were used for mutagenesis.

Q581W, 5'-GGA GAG GAA GAC ATT TGG GAA GCT CCA GAG GAG-3'

E591W, 5'-GAG GCC ACT GAC ACA TGG GTT CCT AAG AAG AAG-3'

R601W, 5'-AAG AAA GGA TTC TTC TGG CGG GCC TAT GAC CTG-3'

D611W, 5'-CTG TTT TGT GGG CTG TGG CAG GAT AAG GGA CCC-3'

E621W, 5'-CCC AAG ATG ACC AAG TGG GAG GAG GCT GCC ATG-3'

L630W, 5'-GCC ATG AAG CTG AAG TGG ACA GAC ACC TCC GAG-3'

The *Apa*I site (underlined) was silently introduced in a selection primer as an aid in screening with the oligonucleotide primer:

5'-GCA AAT CGC GCT GTT AGC GGG ACC ATT AAG TTC TGT CTC GGC-3'.

The mutant cDNAs were sequenced to verify desired mutations at various points. The confirmed cDNA's were ligated into pGEX-4T-1 expression vector. The recombinant plasmids were then transformed into BL21 (DE3) cells for expression of wild type and Trp mutants of loop 13.

3.4. Peptide Expression and Purification

Amino terminal GST tag peptides of wild type and all mutants were expressed in *Escherichia coli* cells in *Lauria-Bertani* (LB) medium supplemented with 100 μg/ml ampicillin as an antibiotic. Expression of the peptides was induced by addition of 1 mM isopropyl-β-D-thiogalactopyranoside for 3.5 h at 37 °C in a 2 L culture. Cells were pelleted by centrifugation at 8 000 *rpm* for 10 min at 4 °C; resuspended in 20 mL of PBS lysis buffer [140 mM NaCl, 2.7 mM KCl, 10 mM Na_2HPO_4 and 1.8 mM KH_2PO_4 (adjusted to pH 7.4)] supplemented with 5 mM DTT, 0.1% Triton X-100, 1 mg/ml lysozyme, and Protease Inhibitor Cocktail (one tablet). Cells were effectively lysed using a SONOPULS Ultrasonic Homogenisation system under mild conditions. The lysate was centrifuged at 17 000 *rpm* for 45 min at 4 °C. The supernatants containing GST tag peptides were applied to glutathione-Sepharose columns

(Amersham Biosciences, Freiburg, Germany) after being passed through a 0.2 μM filter. Soluble fractions of wild type and Trp mutants of loop 13 (amino acid residues 564-638) after removal of the protease inhibitor were generated by treating the glutathione-Sepharose-immobilized fusion peptide, derived from pGEX-4T-1, with 2 units/ml of thrombin in PBS for 16 h at 4 °C. The purity of wild type and all mutants was assessed by SDS-PAGE using a precasted Bis-Tris 4-12% gel in Tris-glycine running buffer and staining with Coomassie Blue. The purity of the peptides was at least 90%. All peptide concentrations were determined by the method of Lowry using bovine serum albumin as a standard (Lowry *et al*., 1951).

3.5. Circular Dichroism Analysis

The far-UV CD spectra were recorded between 190 and 250 nm (350 μl sample volume) on a Jasco J-715 spectropolarimeter equipped with a temperature-controlled incubator at 20 °C using quartz cells of 1 mm optical path length and 10 μM of wild type loop 13. The step size was 0.5 nm with a 1.0-nm bandwidth at a scan speed of 50 nm/min. An average of 10 scans was obtained for blank and peptide spectrum, and the data was corrected for buffer contributions. The measurements were performed under nitrogen flow. The secondary structure percentages were calculated using the K2d computer modeling program. The results were expressed as mean residue ellipticity in units of degrees/cm^2/dmol. The spectrum was recorded in 10 mM phosphate buffer at pH 6.8.

3.6. Photoaffinity Labeling of Loop 13 with (2'-Azi-*n*-Octyl)-β-D-Glucoside

Photoaffinity labeling was performed with the photolabile alkyl glucoside analogue, (2'-Azi-*n*-octyl)-β-D-glucoside, as previously reported (Gibbs *et al*., 1982; Lin *et al*., 1982). The photolabeling experiments were carried out in 100 μl PBS buffer (pH 7.4) containing 225 μg wild type loop 13 peptide and 1 mM (2'-Azi-*n*-octyl)-β-D-glucoside. The mixture was preincubated at room temperature in the dark for 5 min. After incubation, photolysis was carried out in a Rayonet photochemical reactor RPR-100 (Southern New England Ultraviolet Co., Branford, CT,) fitted with sixteen, 2800-

Å lamps at 22 °C for 10 min. As a control, the photoprobe was first exposed to UV light and then added to the peptide. No labeling was observed in the absence of UV light. After photoaffinity labeling the peptide was precipitated with chloroform methanol (v/v 2:1). A small part of the peptide pellet was solubilized with 0.1% trifluoroacetic acid in 50% acetonitrile for MALDI-TOF mass spectrometry analysis and the rest of the peptide pellet was dissolved in sample buffer for SDS-PAGE. The peptide was separated by SDS-PAGE using NuPAGE 4-12% BisTris Gels (Invitrogen). Gel was stained with Coomassie Brilliant Blue G-250 (Neuhoff *et al*., 1985). Bands of interest were excised from a gel with a clean razorblade, sliced into 1-mm^3 cubes, incubated over night at room temperature with 200 μl of 50 mM NH_4HCO_3, pH 8.5, 50% acetonitrile, dehydrated with 200 μl acetonitrile, and dried in a centrifugal evaporator. Gel pieces were rehydrated with a small volume of digestion solution (50 mM NH_4HCO_3, 5 mM $CaCl_2$, and 12.5 ng/μl of trypsin) at 4 °C for 30 min. Trypsin was used at an enzyme/substrate ratio of ~ 1:100 by weight. Digestion was allowed to proceed overnight at 37 °C. Peptides were extracted from the gel pieces with 100 μl of 20 mM ammonium bicarbonate, followed by 2 extractions of 1:1 water/acetonitrile plus 1% trifluoroacetic acid and one extraction with 100 μl of acetonitrile. Each extraction step was carried out after incubation of samples for 10 min at room temperature. All extracts were combined in a fresh tube, flash-frozen, and dried in a centrifugal evaporator. Dried extracts were stored at -20° C until analyzed. Mass spectra were acquired in the positive ion, linear mode on a Voyager DE-PRO MALDI (PE-Biosystems, Shelton, CA). After mixing the solubilized peptide with 2,5-dihydroxybenzoic acid matrix (saturated 2,5-dihydroxybenzoic acid solution in 0.1% trifluoroacetic acid in 50% acetonitrile) for intact loop 13 peptide, and for acquisition of a mass spectrometric peptide map of the trypsin digested peptide, 0.5-μl aliquots of the generated cleavage products were dispensed onto the sample support, followed by 0.5 μl of α-cyano-4-hydroxycinnamic acid matrix solution (solution of α-cyano-4-hydroxycinnamic acid in 0.1% trifluoroacetic acid in 50% acetonitrile). Samples were deposited on a MALDI plate and dried at room temperature prior to collecting the spectra.

3.7. Preparation of Lipid Vesicles

Chloroform solutions of DOPC and DOPG (10 mg/ml stock solution) were mixed to obtain 70:30 and 60:40 percent molar ratios of zwitterionic and negatively charged lipids, respectively. The lipid mixtures were dried under a gentle stream of nitrogen for 3 h. To the dried phospholipid film, PBS (pH 7.4) was added at 35 °C to a final concentration of 2 mg/ml and the glass tube was covered with parafilm. After 1 hr, the phospholipids were vigorously shaken. Small unilamellar vesicles (SUVs) were prepared by sonication in a bath sonicator, applying cycles of 5 min pulse at 3 min interval for ~2 h above the transition temperature (Tc) of the lipids to get a nearly clear solution. A homogenous liposome size distribution of ~75 nm was confirmed by dynamic light scattering analysis, using a Dynamic Light Scattering ISS720 device. SUVs were freshly prepared for all reconstitution studies.

3.8. Preparation of Peptide-Lipid Vesicles

The peptide-lipid complexes were prepared in clean small glass test tubes in 500 μl volume. After mixing 3 μM of each mutant with lipid vesicles (150 μM), the reaction mixture was further sonicated applying 2-3 cycles of 3 min pulse at 2 min interval. The reaction mixture was incubated at room temperature for 10 min. All samples were then transferred to 0.3 cm quartz cell to collect the emission spectra.

3.9. Steady State Trp Fluorescence

The fluorescence experiments were performed using a Perkin-Elmer LS 50B fluorescence spectrometer (Perkin-Elmer), fitted with a 450W xenon arc lamp at room temperature. A 0.3-cm excitation and emission path length quartz cell was used for all the fluorescence measurements. The excitation wavelength was set at 295 nm for selective excitation of Trp. A 290 nm cutoff filter was used to minimize the contribution of scattering signals. Emission spectra were collected from 300-400 nm, averaging six scans. The bandwidths for both excitation and emission monochromators were 5 nm. The emission spectra were corrected for background and dilution effects.

3.10. Ligand Binding Assay

3.10.1. Binding of Phlorizin/Phloretin to Single Trp Mutants

The ligand-induced fluorescence quenching as a function of phlorizin or phloretin concentration was monitored as described (Xia *et al*., 2003). Increasing amounts of phlorizin or phloretin (from 1 to 650 μM) were added to all Trp mutants (5 μM) in PBS. Briefly, as increasing amounts of phlorizin or phloretin were added, the fluorescence intensity decreased. Apparent binding constants were calculated from titration data by determining the percentage of quenching at saturating phlorizin or phloretin concentrations using single-site binding equation in a non-linear regression analysis program, Prism (Graphpad, San Diego, CA).

3.10.2. Binding of n-Hexyl-β-D-Glucoside to Single Trp Mutants

Fluorescence quenching was observed in the presence of various concentrations of n-hexyl-β-D-glucoside for each mutant. This signal was utilized to calculate the dissociation constants. Increasing amounts of *n*-hexyl-*β*-D-glucoside (from 1 to 350 μM) were added to all mutants (5 μM) in PBS (pH 7.4). The corrected relative fluorescence intensity at different ligand concentrations was determined. Apparent binding constants were calculated using a single-site binding equation in the non-linear regression analysis program, Prism (Graphpad, San Diego, CA).

3.11. Fluorescence Quenching by Acrylamide

3.11.1. Effect of Phlorizin/Phloretin on Acrylamide Quenching of Trp Mutants

Acrylamide-dependent Trp fluorescence quenching experiments were performed in PBS (pH 7.4) for wild type and mutant peptides (5 μM) in the absence and presence of 50 μM phlorizin or phloretin. Acrylamide was added from aliquots of an 8 M stock solution to each peptide solution (25 °C) up to 500 mM. The peptides were incubated with the substrate at room temperature for 2 min prior to collecting the fluorescence spectra. The accessibility of Trp was monitored by analysing the quenching data using

a Stern-Volmer equation: $F_0/F = 1 + K_{SV}$ [Q] (Lackowicz, 1999), where F_0 is the fluorescence of the peptide in the absence of quencher and F is the observed fluorescence at the concentration of the quencher ([Q]). K_{SV} is the collisional quenching constant which was determined from the slope of best fit values of Stern-Volmer plots at a given concentration of the quencher. The difference between inner filter effects of substrate (50 μM) from the titration of L-Trp (5 μM) performed at an excitation of 295 nm and emission at 355 nm was found to be much less and hence was not considered in our measurements.

3.11.2. Effect of Various Alkyl Glucosides on Acrylamide Quenching of Trp Mutants

Trp fluorescence quenching experiments were performed in PBS (pH 7.4) for all Trp mutants (5 μM) in the absence and presence of 30 μM of *n*-hexyl-β-D-glucoside, *trans*-*n*-3-hexenyl-β-D-glucoside, *cis*-*n*-3-hexenyl-β-D-glucoside, *n*-octyl-β-D-glucoside, *n*-decyl-β-D-glucoside or 1-hexanol. Acrylamide was added at room temperature as aliquots from a 5 M stock solution to each mutant peptide solution up to 350 mM. The accessibility of each Trp was monitored by analysing the quenching data using a Stern-Volmer equation as described in section 3.11.1. The difference between inner filter effects of the ligands found for the titration of a L-Trp solution (5 μM) at an excitation of 295 nm and emission at 355 nm was found to be much less and hence was not considered further in our measurements.

3.11.3. Effect of Lipid Vesicles on Acrylamide Quenching of Trp Mutants

Acrylamide quenching experiments were carried out at an excitation wavelength of 295 nm to reduce the absorbance by acrylamide. Small aliquots of acrylamide were added from 5 M stock solution up to 350 mM to 3 μM of each Trp mutant in the absence and presence of pure PC and PC/PG (60:40 and 70:30 % molar ratios, respectively) vesicles at 150 μM lipid concentration. All measurements were performed in PBS (pH 7.4). The data were analysed according to the Stern-Volmer equation as described in section 3.11.1.

4. RESULTS

4.1. Expression and Purification of Wild Type and Mutant Peptides

Peptides were expressed in *Escherichia coli* and purified with a yield of ~2.5mg/L culture. Plasmid pGEX-4T-1 containing wild type loop 13 generates a Trp-free peptide, thus the introduced Trp is the only reporter group for each of the mutant peptides. To determine whether the correct product was expressed, MALDI-mass spectrometry was performed which shows the mass peak at *m/z* 8689.56 as expected for loop 13 on the basis of the amino acid sequence (Figure 4.1A). The purity of all single Trp mutants was assessed by SDS-PAGE (Figure 4.1B).

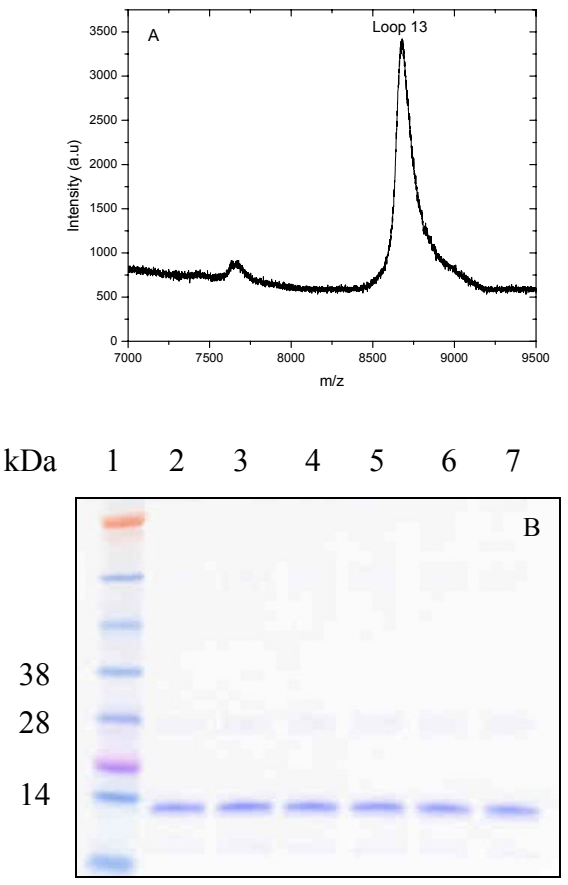

FIG. 4.1. Purification of Wild type and single Trp mutants of loop 13 (564-638 amino acid residues). A, MALDI-mass spectrometry of loop 13. **B,** Coomassie Blue-stained polyacrylamide gel of the GST cleaved peptides (10 μg/lane). Lane 1; Protein standard (kDa), Lane 2-7; six single Trp mutants (~9 kDa) after trypsin digestion of GST fusion protein.

4.2. Secondary Structure of Loop 13 as Determined by CD Analysis

The Circular Dichroism (CD) spectrum of loop 13 at pH 6.8 is shown in Figure 4.2. The CD spectrum shows characteristic minima at 222 and 208 nm from which the secondary structure was estimated to consist of 37% α-helical residues and 63% random coil.

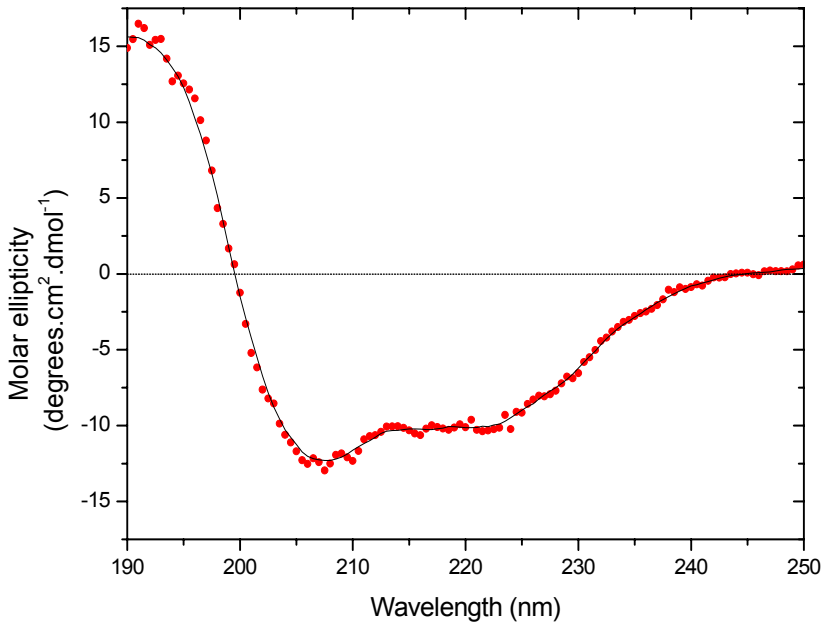

FIG. 4.2. Secondary structure of loop 13 as revealed by CD spectroscopy. CD spectrum was recorded as described under "Experimental Procedures." The measurement was carried out at 10 μM peptide concentration in 10 mM phosphate buffer (pH 6.8) at 20 °C.

4.3. Computer Modeling of Loop 13

To predict the secondary structure of loop 13 determined by CD analysis, the computer-modeling program PSIPRED (McGuffin *et al.*, 2000) was used which is shown in Figure 4.3 as a graphical output prediction. The program predicts about 40% α-helical residues and 60% random coil, while no beta strands were detected in the peptide. The 75 amino acids of loop 13 are shown in the form of amino acid codes.

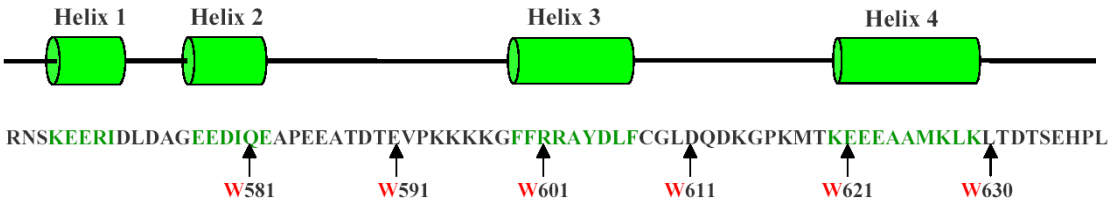

FIG. 4.3. Primary sequence analysis of loop 13 by computer-modeling program PSIPRED. The predicted α-helices are shown in *green*. *Black* lines represent the random coil of loop 13. The sequence of loop 13 is shown from amino acid residues 564 to 638. The positions of six single-Trp residues are shown in *red*.

4.4. Positions of Six Single Trp-Mutations on Loop 13

Site-specific mutations were performed to introduce single Trp residues at six different positions of the molecule which are shown in Figure 4.3. The single mutations at the six positions of the molecule did not affect the structure of loop 13 significantly as determined by computer modeling primary sequence analysis of all Trp mutants (not shown). The derived model was further exploited to determine the sequence specific interaction between inhibitor and Trp mutants of loop 13 by fluorescence measurements (see section 4.5).

4.5. Interaction of Phlorizin with Loop 13

4.5.1. Effect of Phlorizin on Trp Fluorescence

4.5.1.1. Mutants Q581W and E591W: Fluorescence and Effect of Phlorizin

The corrected spectra of Trp fluorescence (λ_{ex} = 295 nm) of Q581W and E591W are shown in Figure 4.5.1 (black lines). The emission maxima of both Trp mutants are in the range of 348–350 nm, which is typical for a hydrophilic environment. 100 μM phlorizin was used to monitor the percentage of quenching regarding the various positions of each Trp mutant. The effects of phlorizin on these mutants are compiled in Figure 4.5.1 (red lines) and Table 4.5.1.

4.5.1.2. Mutants R601W, D611W, E621W and L630W: Fluorescence and Effect of Phlorizin

The corrected Trp fluorescence spectra of R601W, D611W, E621W, and L630W are shown in Figure 4.5.1 (black lines). The fluorescence maxima for these proteins are in the range of 341–343 nm, indicating a slightly less polar environment compared with Q581W and E591W. The effects of phlorizin on these mutants are compiled in Figure 4.5.1 (red lines) and Table 4.5.1.

The differences between the fluorescence quenching spectra of the various mutants suggest that different segments of loop 13 react differently to the binding of phlorizin to the loop. Such differences could, however, also be due to differences in the phlorizin affinity of the mutants. We therefore determined the apparent binding affinities (section 4.5.2).

Table 4.5.1. Comparison of the Effect of Phlorizin on Trp Fluorescence of Each Single Trp Mutant (as shown above).

Peptide	Fluorescence Intensity (%)			Fluorescence maxima (nm)		
	No [a]	phlorizin	Δ (quenching)	No	phlorizin	Δ (shift)
Q581W	100	46	54	348	351	+3
E591W	100	42	58	349	355	+6
R601W	100	33	67	342	350	+8
D611W	100	20	80	341	355	+14
E621W	100	35	65	343	354	+11
L630W	100	82	18	343	353	+10

[a] The values are the percentage of fluorescence yield in the absence of phlorizin
Δ Delta represents the differences between the values
\+ Represents a red shift in maxima

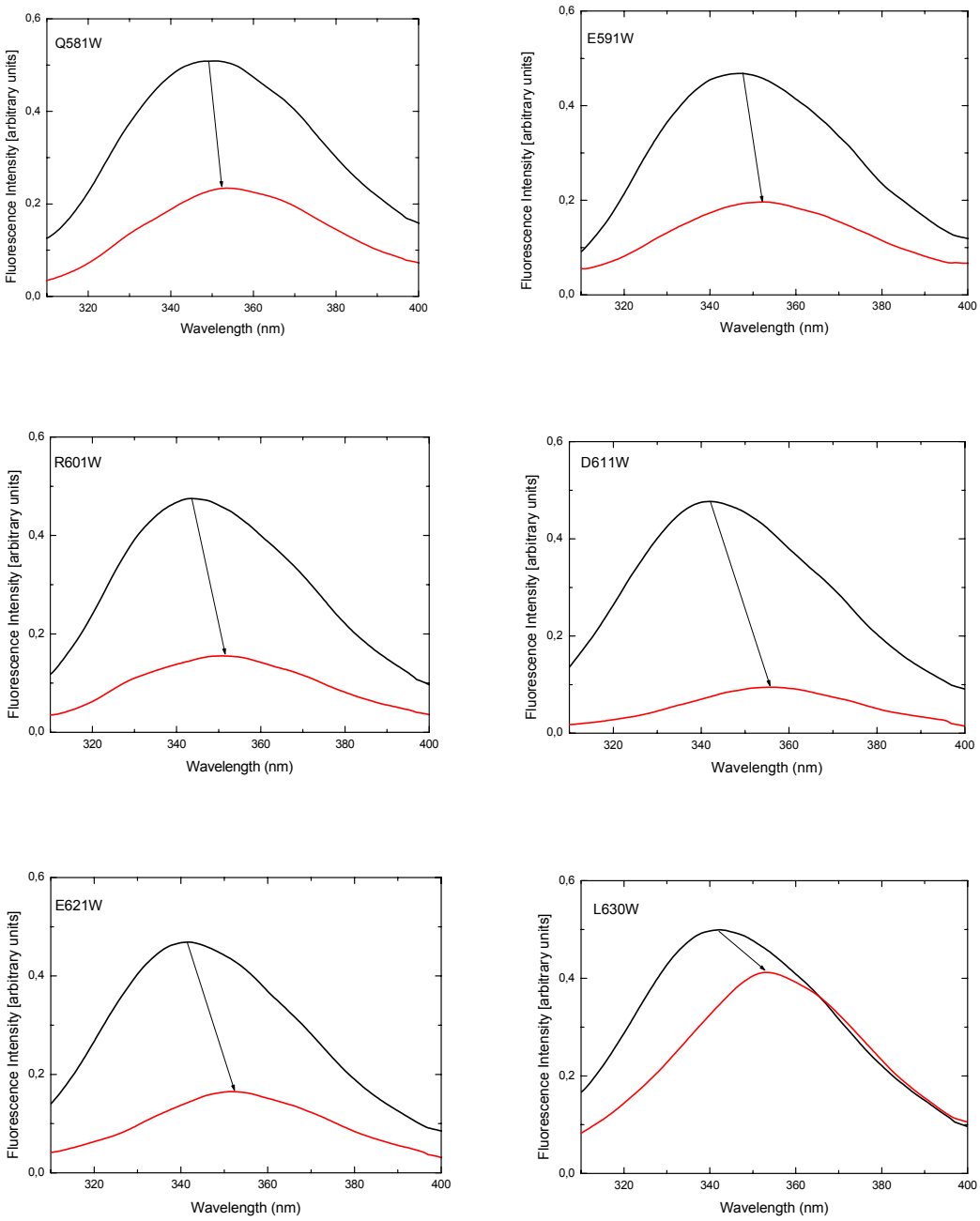

FIG. 4.5.1. Effect of phlorizin on fluorescence emission spectra of single Trp mutant peptides. The black lines show the corrected spectra and the red lines represent the effect of 100 μM phlorizin on the intrinsic fluorescence of each Trp mutant. All the spectra were corrected as described under "Experimental Procedures." The percentages of fluorescence quenching for each Trp mutant are presented in the section "Results" and derived from three independent experiments.

4.5.2. Phlorizin Binding to the Trp Mutants

Titration of all single Trp mutants of loop 13 with different concentrations of phlorizin is shown in Figure 4.5.2. About 90% of the fluorescence of each mutant was quenched at the highest concentration of phlorizin. The estimated equilibrium dissociation constants (K_d) for all mutants are presented in Table 4.5.2. For calculation of binding constants, the peak points with shifting toward longer wavelength were collected for each addition of phlorizin.

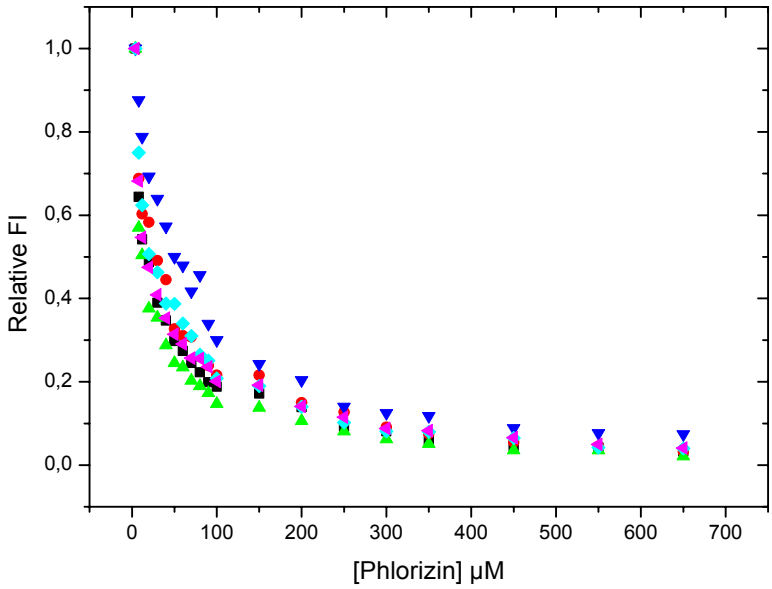

FIG. 4.5.2. Titration of single Trp mutants of loop 13 with phlorizin. All experiments were conducted as described under "Experimental Procedures." Samples include Q581W (■), E591W (●), R601W (▲), D611W (▼), E621W (□), and L630W (◄). The percentage of quenching at saturating phlorizin concentration was calculated from the data and the values were fitted to a single site binding equation using Prism (Graphpad, San Diego, CA) to calculate equilibrium dissociation constants. The K_d values for all mutants are summarized in Table 4.5.2.

The mutant peptides (e.g. Q581W, E591W, R601W, E621W and L630W) showed values very similar to the wild type loop 13 (Xia *et al*., 2003) indicating that the replacement of amino acids at these positions by Trp residues does not change the ability of the peptide to bind phlorizin. There is, however, a lower affinity of mutant peptide D611W which is consistent with the mutagenesis studies on the whole protein.

Table 4.5.2. Apparent Affinity of Phlorizin to the Single Trp Mutants of Loop 13

Parameters of phlorizin binding were derived from the data shown in Figure 4.5.2.

Peptide	K_d (μM)
Q581W	18 ± 2
E591W	25 ±11
R601W	15 ± 7
D611W	54 ± 12
E621W	26 ± 8
L630W	19 ± 5

Values are the mean ± standard deviation of two or three independent experiments.

4.5.3. Effect of Phlorizin on Trp Accessibility to Collisional Quenching

The collisional quencher acrylamide was used to detect changes in the 'accessibility' of Trp to the surrounding solvent. The Stern-Volmer quenching plots of each mutant in which F_0/F is plotted against the acrylamide concentration in the presence and absence of phlorizin were linear and are shown in Figure 4.5.3. The Stern-Volmer constants for all mutants are compiled in Table 4.5.3. At 50 μM phlorizin, a non significant protection effect was noted for mutant Q581W. For E591W and R601W mutant peptides the Stern-Volmer constants started to increase and about four to five fold increase by phlorizin was found for D611W. E621W showed less change in quenching and almost no change in quenching was observed for mutant L630W. These data suggest that the major conformational changes are initiated by phlorizin at and/ or in the vicinity of amino acid 611. Furthermore, the accessibility to acrylamide is increased in between the region 591 to 621 by phlorizin suggesting an unfolding of the peptide in this region.

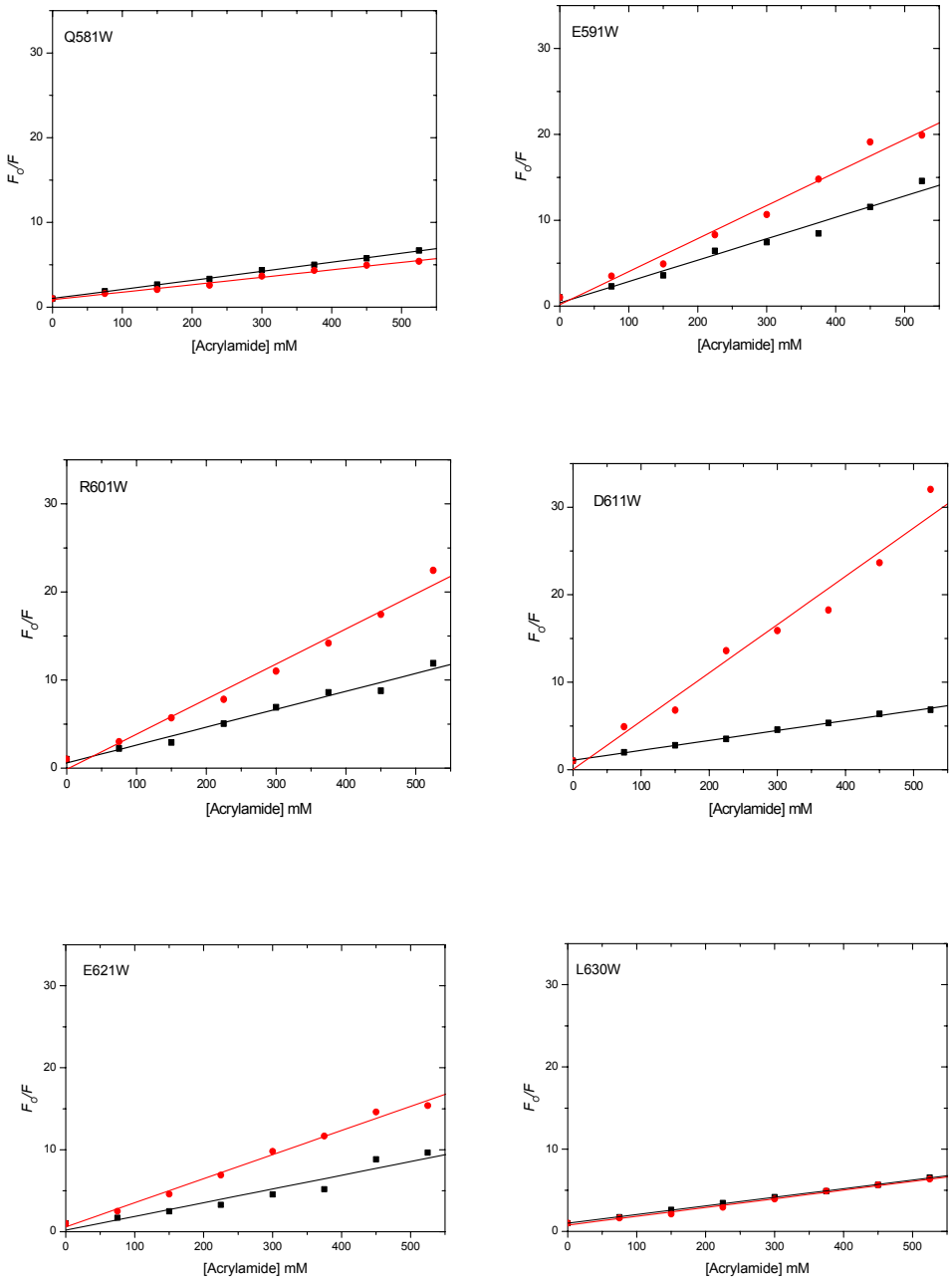

FIG. 4.5.3. Stern-Volmer plots of Trp fluorescence quenching by acrylamide. Quenching experiments were conducted as described under "Experimental Procedures." In each panel the samples were investigated in the absence (■) and presence (●) of 50 μM phlorizin. The slopes of the best fit lines for each data set (K_{SV} values) are shown in Table 4.5.2. Mean values ± standard deviation of two or three independent experiments are given. As a control, 50 μM phlorizin had no effect on acrylamide quenching of L-Trp (5 μM) solution.

Table 4.5.3. Stern-Volmer Constants of Single-Trp Mutants of Loop 13

Fluorescence parameters were determined from the data shown in Figure 4.5.3.

Peptide	Phlorizin [a]	K_{SV} (M^{-1}) [b]
Q581W	-	11 ± 3
	+	9 ± 2
E591W	-	25 ± 4
	+	38 ± 5
R601W	-	20 ± 5
	+	39 ± 4
D611W	-	11 ± 2
	+	55 ± 8
E621W	-	17 ± 3
	+	29 ± 6
L630W	-	10 ± 3
	+	11 ± 4

[a] Quenching experiments were conducted in the absence (-) or presence (+) of 50 μM phlorizin.

[b] The Stern-Volmer quenching constants were determined from the slopes of the lines of $F_0/F = 1 + K_{SV}$ [Q]. Values are the mean ± standard deviation of two or three independent experiments.

4.5.4. Effect of Phloretin and Glucose on Trp Fluorescence and Accessibility to Collisional Quenching

To investigate which part of the glucoside, the sugar or the aglucone, elicited the conformational changes in the peptides, the effect of phloretin, the aglucone of phlorizin, and D-glucose on Trp quenching and accessibility was tested. Experiments were also performed in the presence of phloretin and/or D-glucose for D611W. The corrected spectra of Trp fluorescence (λ_{exc} = 295 nm) of D611W, in the absence and presence of 100 μM phloretin and D-glucose, are shown in Figure 4.5.4 A and C, respectively. The fluorescence of D611W was quenched upon addition of phloretin by 69% with a 9-10 nm red-shift in spectrum. No quenching was observed in the presence of D-glucose. The linear Stern-Volmer quenching plot of D611W in the absence and presence of phloretin is shown in Figure 4.5.4 B. An increase in Stern-Volmer quenching constant for D611W from 11 to 31 M^{-1} was observed. In the presence of 50 μM D-glucose, no significant effect was observed (Figure 4.5.4 D).

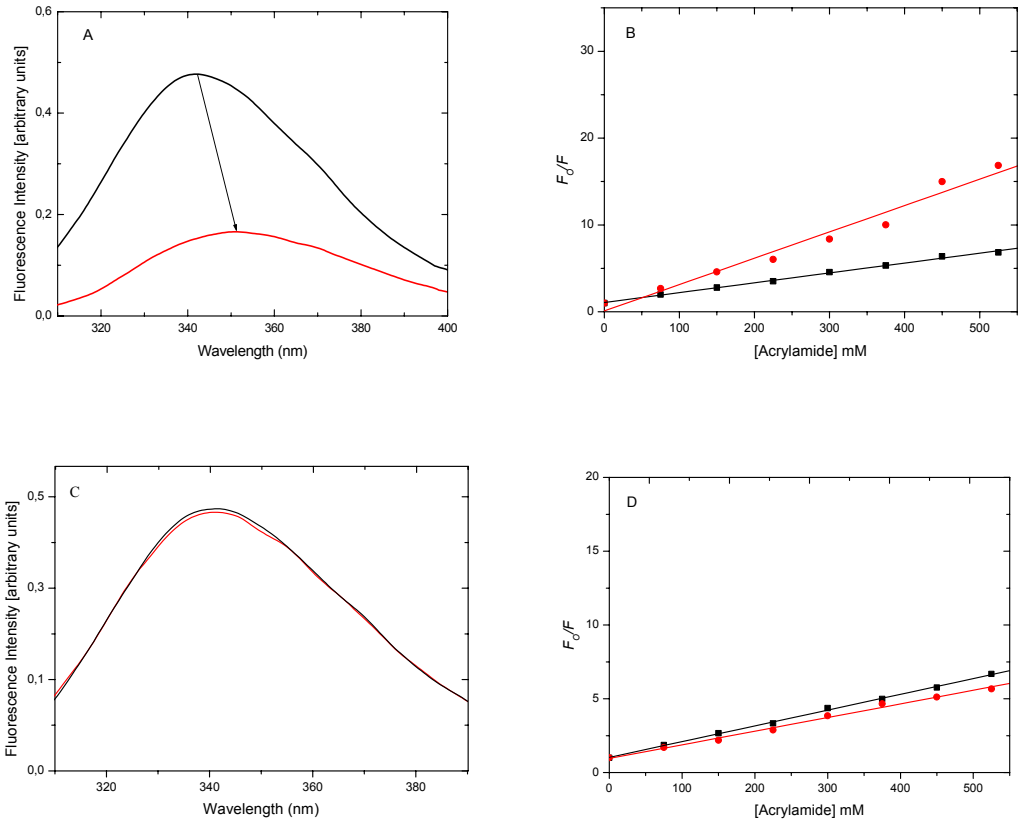

FIG. 4.5.4. Effect of phloretin and D-glucose on fluorescence emission spectrum of D611W. A, The black line shows the corrected spectrum and the red line represents the effect of 100 μM phloretin. **B,** Stern-Volmer plots of Trp fluorescence quenching of D611W by acrylamide in the absence (■) and presence (●) of 50 μM phloretin. **C,** The black line shows the corrected spectrum and the red line represents the effect of 100 μM D-glucose on Trp fluorescence. **D,** Stern-Volmer plots of Trp fluorescence quenching of D611W by acrylamide in the absence (■) and presence (●) of 50 μM D-glucose. The spectra were corrected as described under "Experimental Procedures." Data were derived from two or three independent experiments. Quenching experiments were conducted as described under "Experimental Procedures."

4.6. Interaction of Alkyl Glucosides with Loop 13

4.6.1. Photoaffinity Labeling of Loop 13 with (2'-Azi-n-Octyl)-β-D-Glucoside

In contrast to the phlorizin studies, there was no experimental evidence that alkyl glucosides interact at all with loop 13. We used a photolabeled compound, (2′-Azi-*n*-octyl)-*β*-D-glucoside, which was available in our group to test for an interaction. The photolabeling experiments were performed and analysed by MALDI-mass spectrometry. Figure 4.6.1.1.A shows the expected mass peak for loop 13 at *m/z* 8689.56 before photolabeling. After photoaffinity labeling, an additional peak of *m/z* 9025.28 was observed (Figure 4.6.1.1.B). The mass difference between the first peak (loop 13) and the second peak (*) corresponds to the mass of the photolyzed (2′-Azi-*n*-octyl)-*β*-D-glucoside. Another peak close to *m/z* 7700 was observed which probably represents a degradation product of the peptide. Furthermore, to determine the sites of interaction, photolabeled loop 13 was digested in-gel with trypsin. After extraction of the peptides from the gel, the resulting mixture was analysed by MALDI-TOF. The only additional peak observed in the labeled probe was at *m/z* 845.05 (Figure 4.6.1.2 A and B). This corresponds to an adduct of the peptide Gly-Phe-Phe-Arg of *m/z* 526.27 (amino acid residues 598-601) with the photolyzed (2′-Azi-*n*-octyl)-*β*-D-glucoside (*m/z* 318.78).

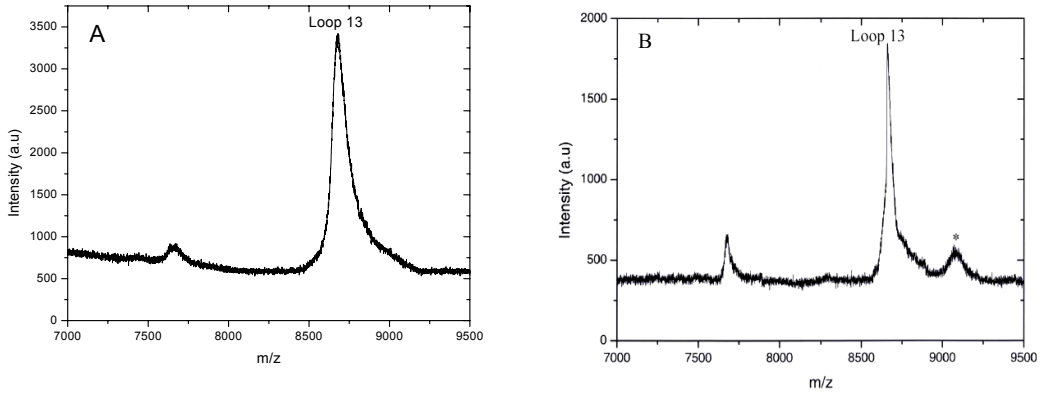

FIG. 4.6.1.1. MALDI-mass spectrometry of photoaffinity-labeled loop 13. Peptide was incubated with (2′-Azi-*n*-octyl)-*β*-D-glucoside in PBS for 5 min in the dark at room temperature, followed by irradiation at 280 nm for 5 min. After separation from noncovalently bound (2′-Azi-*n*-octyl)-*β*-D-glucoside by chloroform/methanol extraction, peptide was dissolved in 2,5-dihydroxybenzoic acid matrix. **(A)** Loop 13 (*m/z* 8689.56) before photoaffinity labeling, **(B)** Loop 13 after photoaffinity labeling. The asterisk denotes loop 13 cross-linked with photolyzed (2′-Azi-*n*-octyl)-*β*-D-glucoside (*m/z* 9025.28). a.u., arbitrary units.

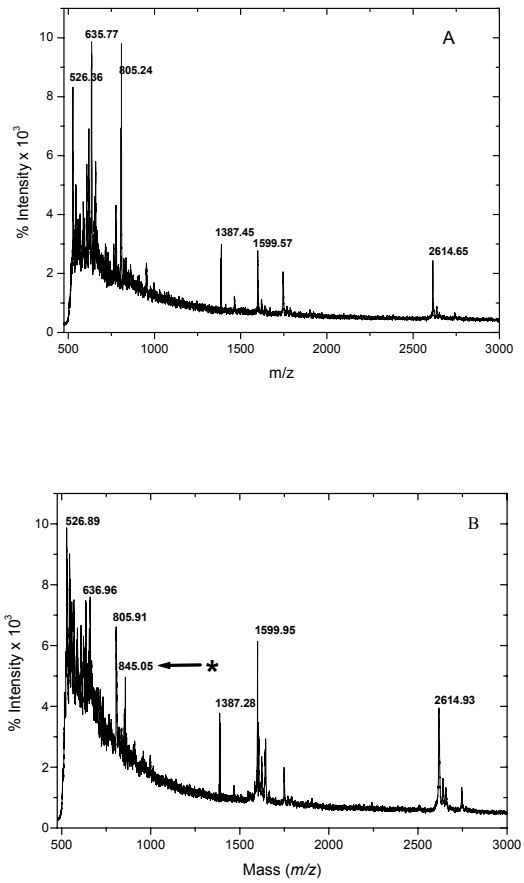

FIG. 4.6.1.2. MALDI mass spectrometry of photoaffinity-labeled loop 13 after in-gel trypsin digestion. The loop 13 was photolabeled with (2′-Azi-*n*-octyl)-*β*-D-glucoside, peptides were separated by SDS-PAGE and peptide bands of interest were excised, destained and digested in gel with trypsin. The peptides were extracted as described under 'Experimental Procedures', and MALDI mass spectra were recorded: **(A)** Loop 13 before photoaffinity labeling, **(B)** Loop 13 after photoaffinity labeling with (2′-Azi-*n*-octyl)-*β*-D-glucoside. The asterisk denotes the additional peak at *m/z* 845.05 which is an adduct of *m/z* 526.27 due to modification of the Gly-Phe-Phe-Arg peptide (amino acid residues 598-601) with photolyzed (2′-Azi-*n*-octyl)-*β*-D-glucoside (*m/z* 318.78).

4.6.2. Effect of n-Hexyl-β-D-Glucoside on Trp Fluorescence

We then tested whether *n*-hexyl-*β*-D-glucoside changed the steady state fluorescence of loop 13 mutants. The corrected Trp fluorescence spectra of Q581W, E591W, R601W, D611W, E621W and L630W in the absence and presence of *n*-hexyl-*β*-D-glucoside are shown in Figure 4.6.2 and compiled in Table Fluorescence quenching and shifts in the maximum were observed for each mutant, although to a different extent.

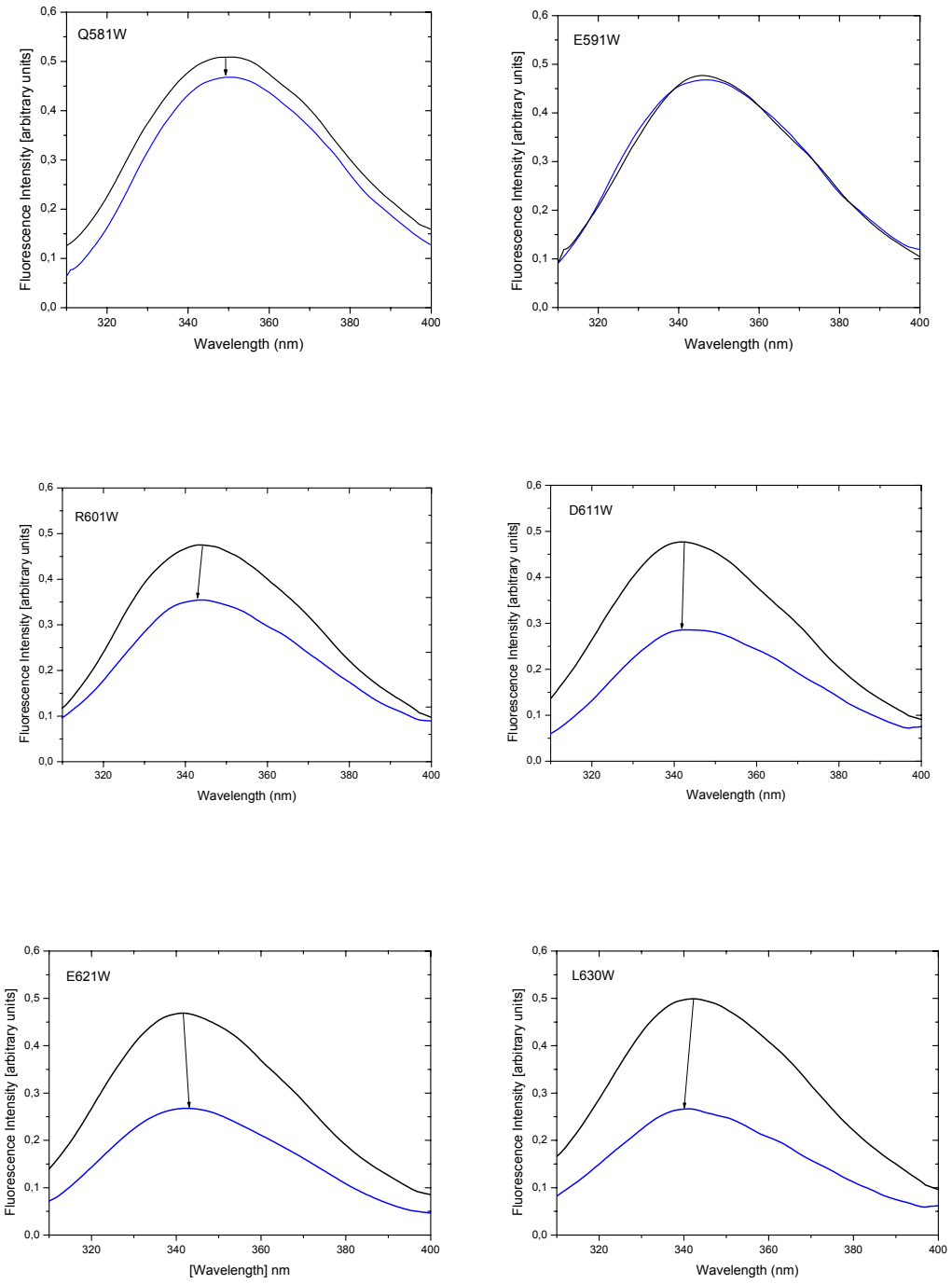

FIG. 4.6.2. Effect of *n*-hexyl-*β*-D-glucoside on fluorescence emission spectra of single Trp mutants of loop 13. The black lines show the corrected spectra in the absence of *n*-hexyl-*β*-D-glucoside, the blue lines represent the effect of 100 μM *n*-hexyl-*β*-D-glucoside on the intrinsic fluorescence.

Table 4.6.1. Summary of the Effect of *n*-Hexyl-β-D-Glucoside on Trp Fluorescence of Each Single Trp Mutant (as shown in Figure 4.6.2).

Peptide	Fluorescence Intensity (%)			Fluorescence maxima (nm)		
	No [a]	*n*-hexyl	Δ (quenching)	No	*n*-hexyl	Δ (shift)
Q581W	100	87	13	348	348	zero
E591W	100	97	3	349	349	zero
R601W	100	74	26	342	343	-1
D611W	100	60	40	341	339	-2
E621W	100	46	54	343	344	+1
L630W	100	54	46	343	340	-3

[a] The values are the percentage of fluorescence yield in the absence *n*-hexyl-β-D-glucoside
Δ Delta represents the differences of the values presented in [a] and [b].
\+ Indicates a red shift in maxima
– Indicates a blue shift in maxima

The differences between the fluorescence quenching spectra of the various mutants, in particular the shifts in the maxima suggest that the various segments of loop 13 react differently to the binding of *n*-hexyl-β-D-glucoside.

4.6.3. Binding of n-Hexyl-β-D-Glucoside to Single Trp Mutants

Affinity of the mutants to *n*-hexyl-β-D-glucoside was determined by titration of the Trp mutants with different concentrations of n-hexyl glucoside, as shown in Figure 4.6.3. Since, we did not observe remarkable changes in Trp fluorescence for Q581W and E591W, the binding affinities were not determined. A maximum quenching of about 55% of the fluorescence was observed for other mutants (R601W, D611W, E621W, and L630W) at high concentrations of *n*-hexyl-β-D-glucoside. The estimated equilibrium dissociation constants for all mutants are presented in Table 4.6.2. They are similar for all mutants and range from 8-14 μM, values comparable to the affinity of *n*-hexyl-β-D-glucoside for the intact SGLT1 in natural membranes (Kipp *et al.*, 1997).

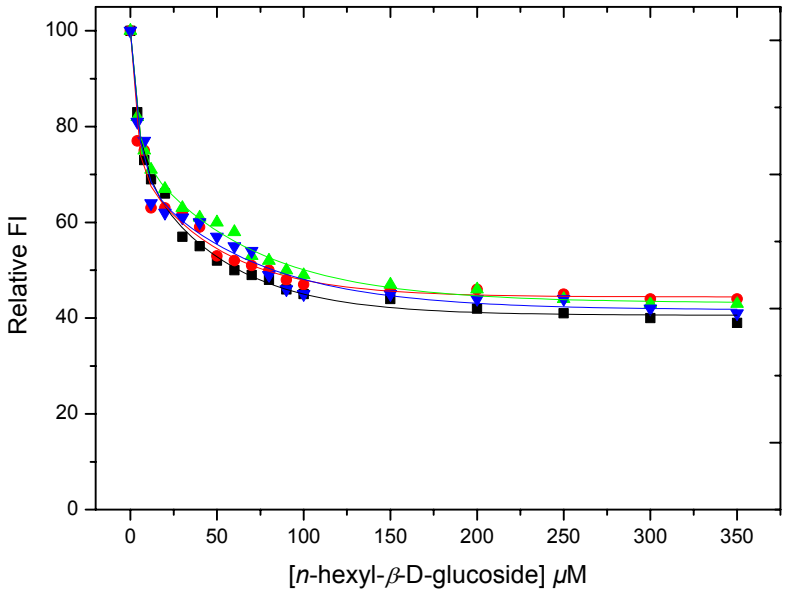

FIG. 4.6.3. Titration of single Trp mutants of loop 13 with *n*-hexyl-*β*-D-glucoside. All experiments were conducted as described under "Experimental Procedures." Samples include R601W (■), D611W (●), E621W (▲) and L630W (▼). The percentage of quenching at high *n*-hexyl-*β*-D-glucoside concentration was calculated from the data and the values were fitted to single site binding equation using Prism (Graphpad, San Diego, CA) to calculate equilibrium dissociation constants. The K_d values for all mutants are summarized in Table 4.6.2.

4.6.4. Effect of n-Hexyl-β-D-Glucoside on Trp Accessibility to Collisional Quenching

The water soluble collisional quencher acrylamide was used to measure the changes in accessibility of each Trp upon *n*-hexyl-*β*-D-glucoside addition. The Stern-Volmer quenching plots in which F_0/F is plotted against the acrylamide concentration in the presence and absence of 30 μM *n*-hexyl-*β*-D-glucoside are shown in Figure 4.6.4. All plots were linear with a regression coefficient higher than 0.99. The Stern-Volmer constants for all mutants are compiled in Table 4.6.2. Maximum decrease in accessibility was noted for mutant R601W, slight protection was observed for D611W and L630W. In contrast, a slight increase in Trp accessibility was found for E621W.

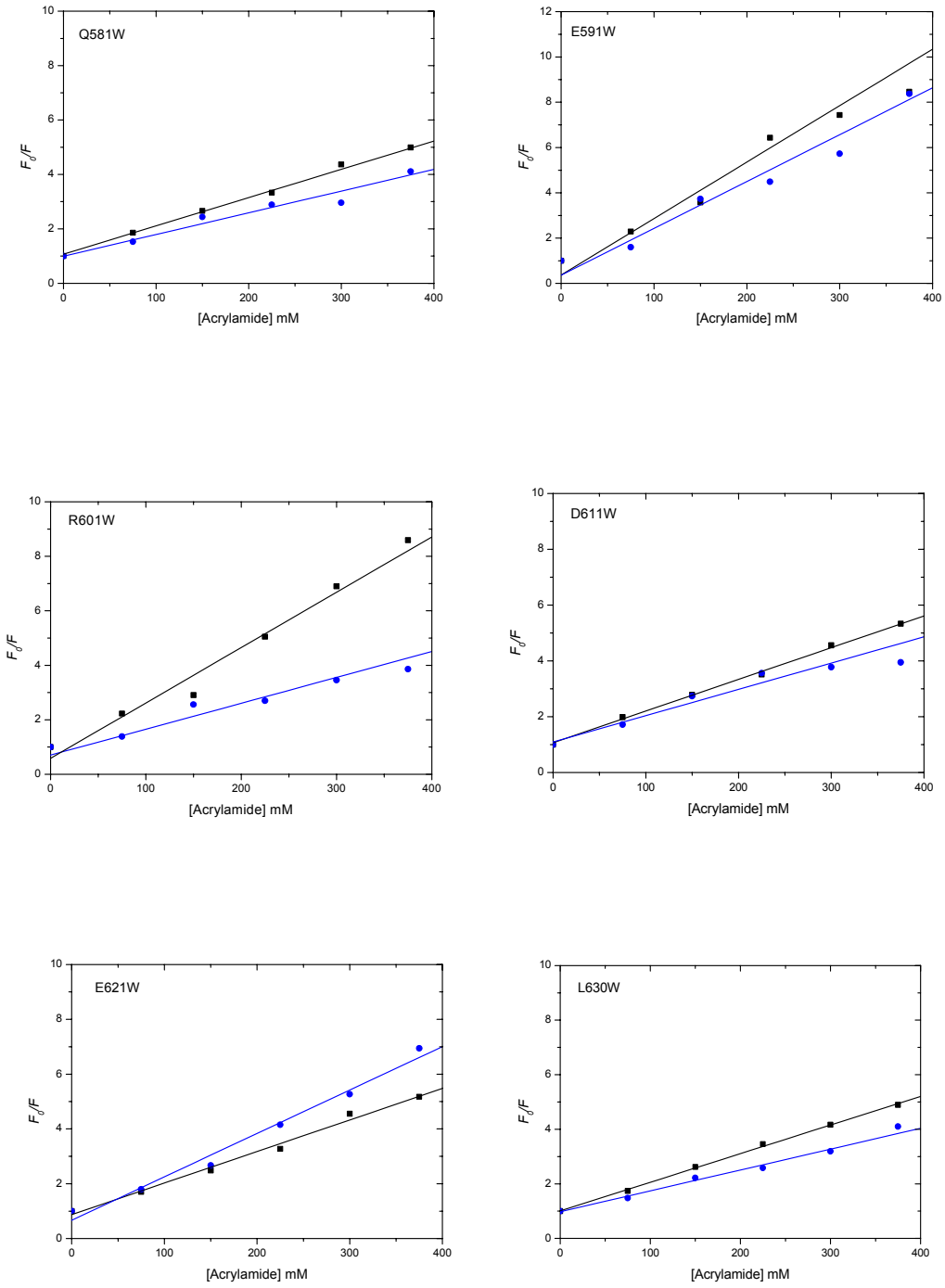

FIG. 4.6.4. Stern-Volmer plots of Trp fluorescence quenching by acrylamide. Quenching experiments were conducted as described under "Experimental Procedures." In each panel the samples were investigated in the absence (■) and presence (●) of 30 μM *n*-hexyl-β-D-glucoside. The slopes of the best fit linear regression lines for each data set (K_{SV} values) are shown in Table 4.6.2.

Table 4.6.2. Acrylamide Accessibility and Apparent Affinity of *n*-Hexyl-β-D-Glucoside to the Single-Trp mutants of Loop 13[a]

Peptide	*n*-hexyl-β-D-glucoside [b]	K_{SV} [c] (M^{-1})	K_d [d] (μM)
Q581W	-	11 ± 2	-
	+	9 ± 2	
E591W	-	21 ± 3	-
	+	19 ± 4	
R601W	-	21 ± 3	12 ± 4
	+	8 ± 1	
D611W	-	11 ± 2	8 ± 3
	+	8 ± 2	
E621W	-	12 ± 3	14 ± 6
	+	16 ± 2	
L630W	-	11 ± 1	9 ± 2
	+	8 ± 1	

[a] Parameters of *n*-hexyl-β-D-glucoside binding and acrylamide accessibility were derived from the data shown in Figures 4.6.3 and 4.6.4, respectively.

[b] Quenching experiments were conducted in the presence (+) or absence (-) of 30 μM *n*-hexyl-β-D-glucoside.

[c] The Stern-Volmer constants were determined from the slopes of the linear regression lines from plots of $F_0/F = 1 + K_{SV}$ [Q]. Values are mean ± standard deviation of two or three independent experiments.

[d] The apparent equilibrium dissociation constants (K_d) are means ± standard deviation of two or three independent experiments.

4.6.5. Stereo-selectivity of the Interaction of Alkyl Glucosides with Loop 13

In intact brush border membranes, a distinct stereo-selectivity was observed for the interaction of alkyl glucosides with SGLT1 (Kipp *et al*., 1996). The position of the residue at C1 (β versus α), the conformation after introducing a double bond at C3-C4 (*cis* versus *trans*) and the chain length (C6-C10) turned out to be of importance. We therefore investigated the interaction of the corresponding compounds with loop 13 in vitro. Similar to the studies on intact membranes, the β-glucosides exhibited a more marked change in fluorescence than the α-glucosides, the same holds true for the preference of the *cis* versus the *trans* conformation at C3-C4. Extension of the alkyl chain beyond C6 and C10, however, reduced the responses (see Table 4.6.3.).

4.6.6. Effect of 1-Hexanol on Trp Fluorescence and Accessibility to Collisional Quenching

To investigate which part of the alkyl glucoside, the sugar or the aglucone, is involved in the interaction with loop 13, 1-hexanol and D-glucose were used as ligands. The fluorescence of R601W was quenched upon addition of 100 μM 1-hexanol by 45% with a red shift in maxima by 0.5-1 nm (Figure 4.6.6.A). Also a significant protection effect was observed for 1-hexanol (decrease of K_{SV} to 13 M^{-1} from 21 M^{-1}, Figure 4.6.6.B). No quenching and protection against acrylamide was observed in the presence of glucose as described under Section 4.5.4.

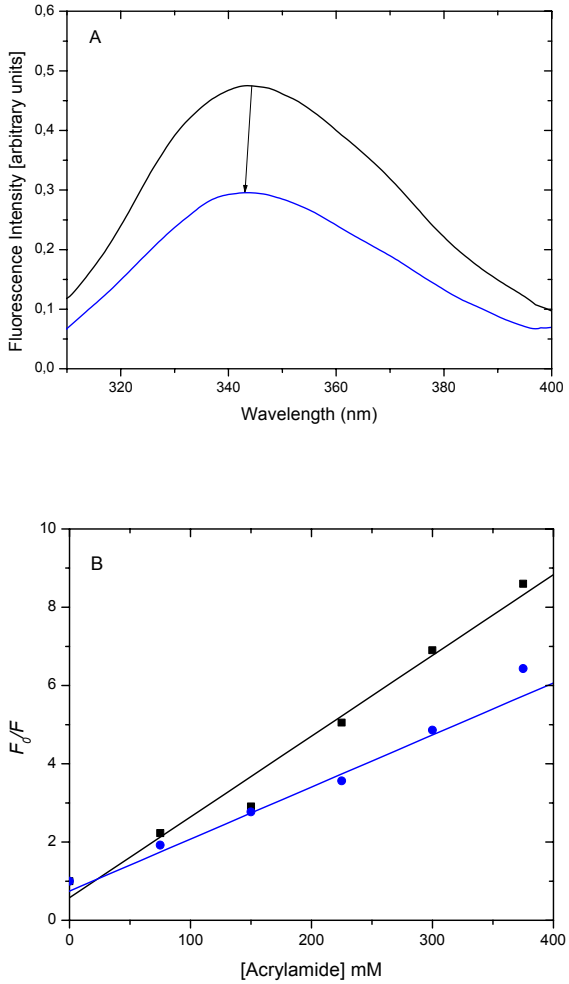

FIG. 4.6.6 **(A)** Effect of 1-hexanol on the fluorescence emission spectrum of R601W. The black lines show the corrected spectrum and the blue lines represent the effect of 100 μM 1-hexanol on intrinsic fluorescence. The spectra were corrected as described under "Experimental Procedures." Data were derived from three independent experiments. **(B)** Stern-Volmer plots of Trp fluorescence quenching of R601W by acrylamide in the absence (■) and presence (●) of 30 μM 1-hexanol. Quenching experiments were conducted as described under "Experimental Procedures."

Table 4.6.3. Effect of Alkyl Glucoside Analogues on Mutant R601W[a]

Glucoside	Quenching [b] (%)		K_{SV} [c] (M^{-1})
n-octyl-β-D-glucoside	35	-	21 ± 3
		+	13 ± 3
n-octyl-α-D-glucoside	3	-	21 ± 3
		+	20 ± 2
trans-*n*-3-hexenyl-β-D-glucoside	20	-	21 ± 3
		+	14 ± 2
cis-*n*-3-hexenyl-β-D-glucoside	28	-	21 ± 3
		+	9 ± 2
n-hexyl-β-D-glucoside	26	-	21 ± 3
		+	8 ± 1
n-decyl-β-D-glucoside	16	-	21 ± 3
		+	18 ± 2

[a] The parameters were derived from the fluorescence quenching data and acrylamide accessibility (not shown).

[b] Values represent fluorescence quenching in the presence of a concentration of each glucoside of 100 μM.

[c] Quenching experiments were conducted in the absence (-) or presence (+) of each glucoside at a concentration of 30 μM.

4.7. Interaction of Loop 13 with Lipid Vesicles

4.7.1. Effect of Lipid Vesicles on Trp Fluorescence

The corrected Trp fluorescence spectra (λ_{exc} = 295 nm) of Q581W, E591W, R601W, D611W, E621W and L630W in the absence and presence of 150 μM DOPC:DOPG (60:40%) are shown in Figure 4.7.1 and compiled in Table 4.7.1. Increase in fluorescence and shifts in the maximum were observed for all mutants, except R601W, although to a different extent.

Table 4.7.1. Summary of the Effect of Vesicles on Trp Fluorescence of Each Single-Trp Mutant (as shown in Figure 4.7.1).

Peptide	Fluorescence intensity (%)	Fluorescence maxima (nm)		
	(increase) [a]	No	PC:PG (60:40%)	Δ (shift)
Q581W	23	348	342	-6
E591W	28	349	347	-2
R601W	zero	342	342	zero
D611W	20	341	340	-1
E621W	17	343	340	-3
L630W	60	343	340	-3

[a] The values are the percentage of increase in fluorescence in the presence of PC:PG (60:40%)

Δ Delta represents the differences between the values

– Indicates a blue shift in maxima

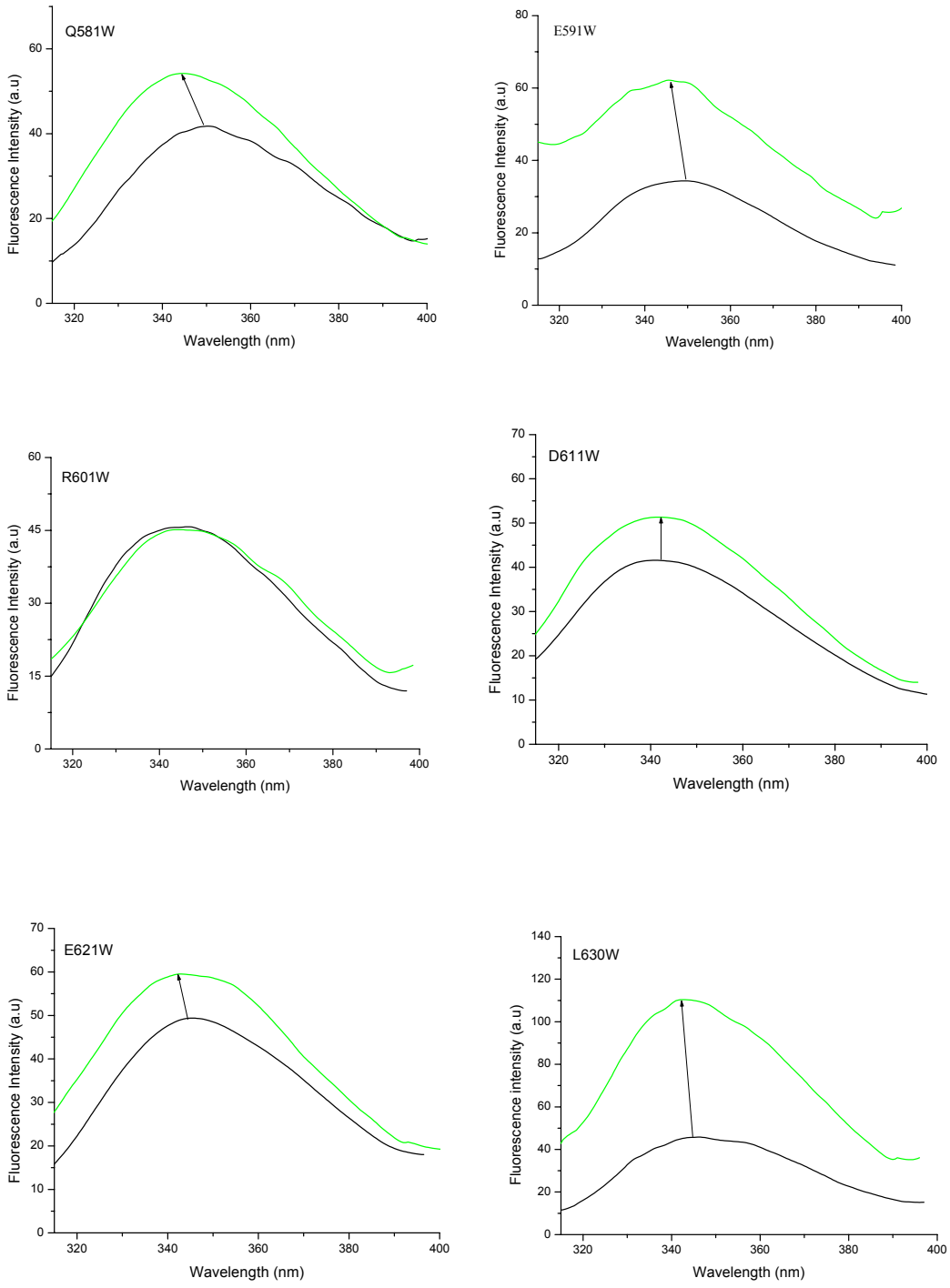

FIG. 4.7.1. Effect of DOPC:DOPG (60:40%) on fluorescence emission spectra of single Trp mutants of loop 13. The black lines show the corrected spectra of Trp mutants (3 μM) in simple buffer (PBS, pH 7.4) and the green lines represent the effect of 150 μM lipid vesicles on Trp fluorescence.

4.7.2. Fluorescence Quenching by Membrane-Embedded Doxyl Spin Labels

The liposome-induced blue shifts and increases in fluorescence intensity of Trp mutants suggest that upon formation of the peptide-lipid complex, the Trp residues Q581W, E621W, and L630W shift to a more hydrophobic environment. This relatively hydrophobic environment could lie either within the protein or in the lipid bilayer. To discriminate between these possibilities, we examined the ability of lipid-embedded nitroxide spin labels to quench the fluorescence of each Trp reporter groups. Only Trp residues that can interact directly with the nitroxide spin groups become quenched. For these experiments, PC:PG (60:40%) vesicles were prepared that contained doxyl-PC labeled at either 5-, or 12-position of the *sn*-2 acyl chain.

All Trp mutants were mixed with constant amount of vesicles containing 50% PC, 10% doxyl-PC, and 40% PG. The spectra from these experiments are shown in Figures 4.7.2.1-4.7.2.3, and the degree of quenching by the nitroxide groups is tabulated in Table 4.7.2. From these spectra, it is apparent that the doxyl-spin labels efficiently quenched Trp at position 621 and 630. Trp fluorescence of E621W is strongly quenched by 5-doxyl spin label and 12-doxyl spin label has almost the same effect on quenching. This would suggest the deep embedding of Trp-621 in the membrane. L630W fluorescence is strongly quenched by 5-doxyl but less quenched by 12-doxyl spin label. The position of this mutant would be suggested to reside deep in the membrane and close to inner bilayer surface than Trp 621 which can also be observed by maximum increase in Trp fluorescence as compared to other mutants. The fluorescence of other mutants was not directly quenched by doxyl-spin labels. Comparatively less quenching of an increased fluorescence induced by PC:PG (60:40%) vesicles was observed for Q581W and D611W by doxyl-spin labels. In addition, no change was observed for R601W.

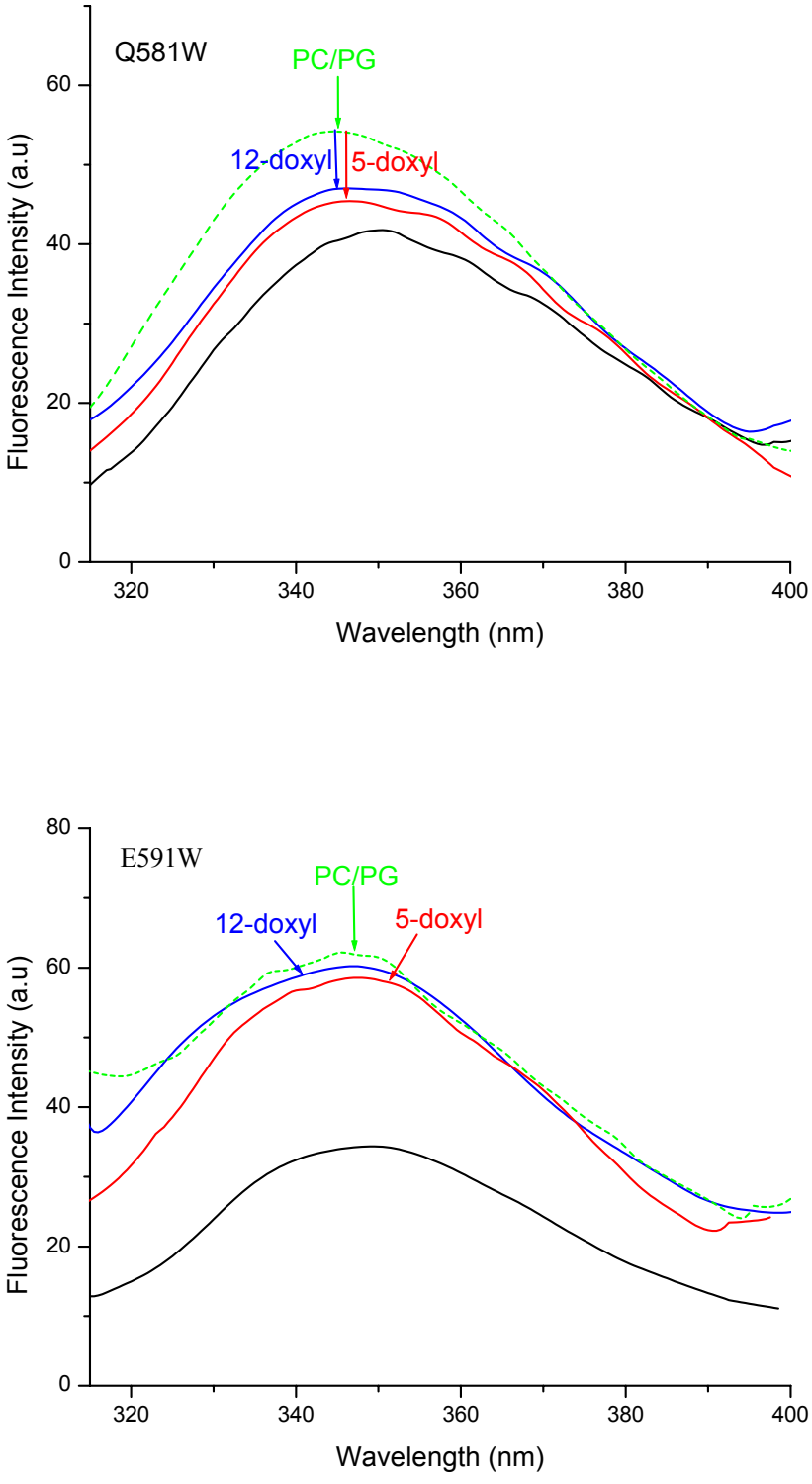

FIG 4.7.2.1. Effect of doxyl-PC on fluorescence emission spectra of Trp mutants Q581W and E591W, respectively. Vesicles composed of 60% PC, 40% PG (dotted green lines) or 50% PC, 40% PG 10% doxyl-PC labeled at either 5- (red), or 12- (blue) position of the *sn*-2 acyl chain were prepared and mixed with mutant peptides (3 μM) in PBS, pH 7.4. The black lines show the corrected spectra in PBS (pH 7.4). All the spectra were corrected as described under "Experimental Procedures." a.u., arbitrary units.

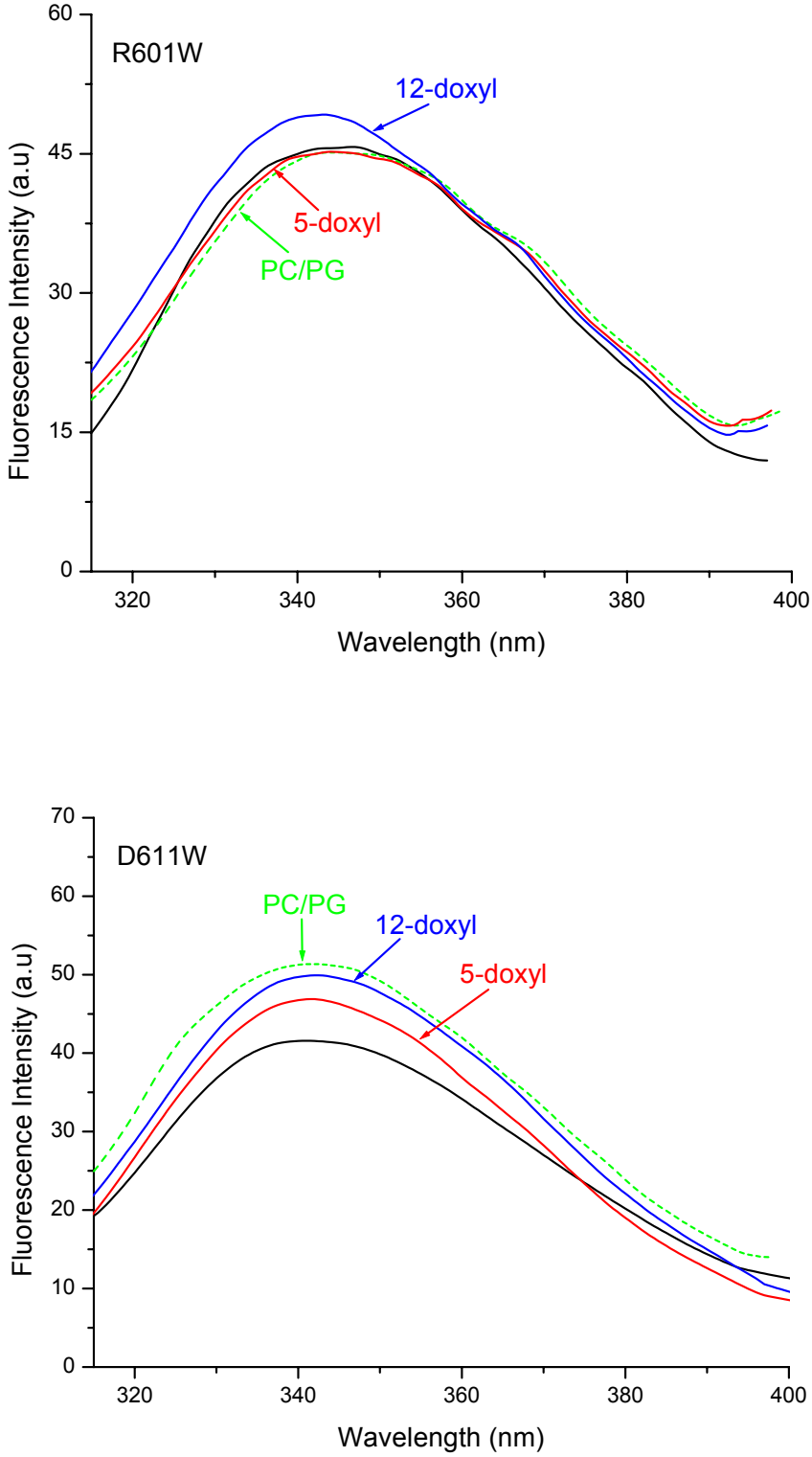

FIG 4.7.2.2. Effect of doxyl-PC on fluorescence emission spectra of Trp mutants R601W and D611W, respectively. Vesicles composed of 60% PC, 40% PG (dotted green lines) or 50% PC, 40% PG 10% doxyl-PC labeled at either 5- (red), or 12- (blue) position of the *sn*-2 acyl chain were prepared and mixed with mutant peptides (3 μM) in PBS, pH 7.4. The black lines show the corrected spectra in PBS (pH 7.4). All the spectra were corrected as described under "Experimental Procedures." a.u., arbitrary units.

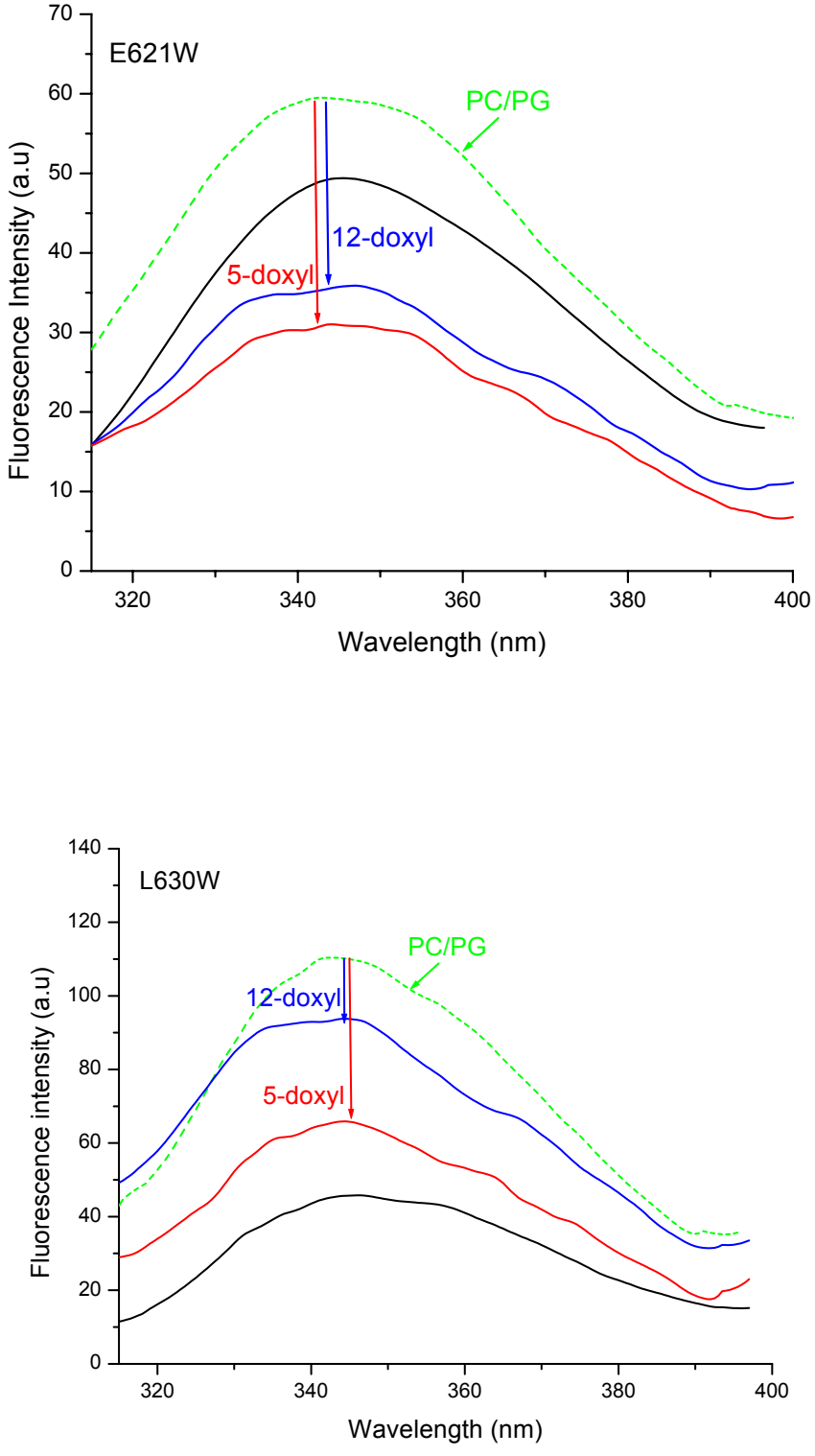

FIG 4.7.2.3. Effect of doxyl-PC on fluorescence emission spectra of Trp mutants E621W and L630W, respectively. Vesicles composed of 60% PC, 40% PG (dotted green lines) or 50% PC, 40% PG 10% doxyl-PC labeled at either 5- (red), or 12- (blue) position of the *sn*-2 acyl chain were prepared and mixed with mutant peptides (3 μM) in PBS, pH 7.4. The black lines show the corrected spectra in PBS (pH 7.4). All the spectra were corrected as described under "Experimental Procedures." a.u., arbitrary units.

Table 4.7.2. Fluorescence Quenching by Membrane-Embedded Doxyl-Spin Labels.

All spectra from Figures 4.7.2.1-4.7.2.3 were integrated and normalized relative to the fluorescence obtained using lipid vesicles (PC:PG) lacking the doxyl-spin label. The percent quenching, relative to the total increase in fluorescence in the presence of PC:PG (60:40%) without nitroxide spin labels, is listed.

Trp Mutants	5-doxyl spin label	12-doxyl spin label
Q581W	14	12
E591W	4	2
R601W	1	-
D611W	9	3
E621W	50	41
L630W	38	14

4.7.3. Effect of Lipid Vesicles on Trp Accessibility to Collisional Quenching

The calculated blue shifts of Trp mutants and quenching by membrane–embedded spin-labeled PC vesicles suggested that some parts of loop 13 might be embedded within the lipid bilayer. This was assessed in a more direct manner by means of acrylamide, a hydrophilic quencher of the Trp fluorescence. In addition, this quencher has the advantage that it has a very low permeability to lipid membranes.

The Stern-Volmer quenching plots of each mutant in the absence and presence of phospholipid vesicles consisting of PC:PG (60:40%) were linear and are shown in Figure 4.7.3. The Stern-Volmer constants for all mutants are compiled in Table 4.7.3. It indicates that the Trp residues are more or less protected against quenching by acrylamide. As expected, Trp-621 and Trp-630 are completely protected. This supports their location in the lipid environment. Surprisingly, Trp-591 despite no interaction with the nitroxide quencher shows strong protection, suggesting an effect of lipid vesicles on folding of the peptide chain. Slight changes are also observed for Trp-581 and Trp-611, Trp-601 appears to be not affected.

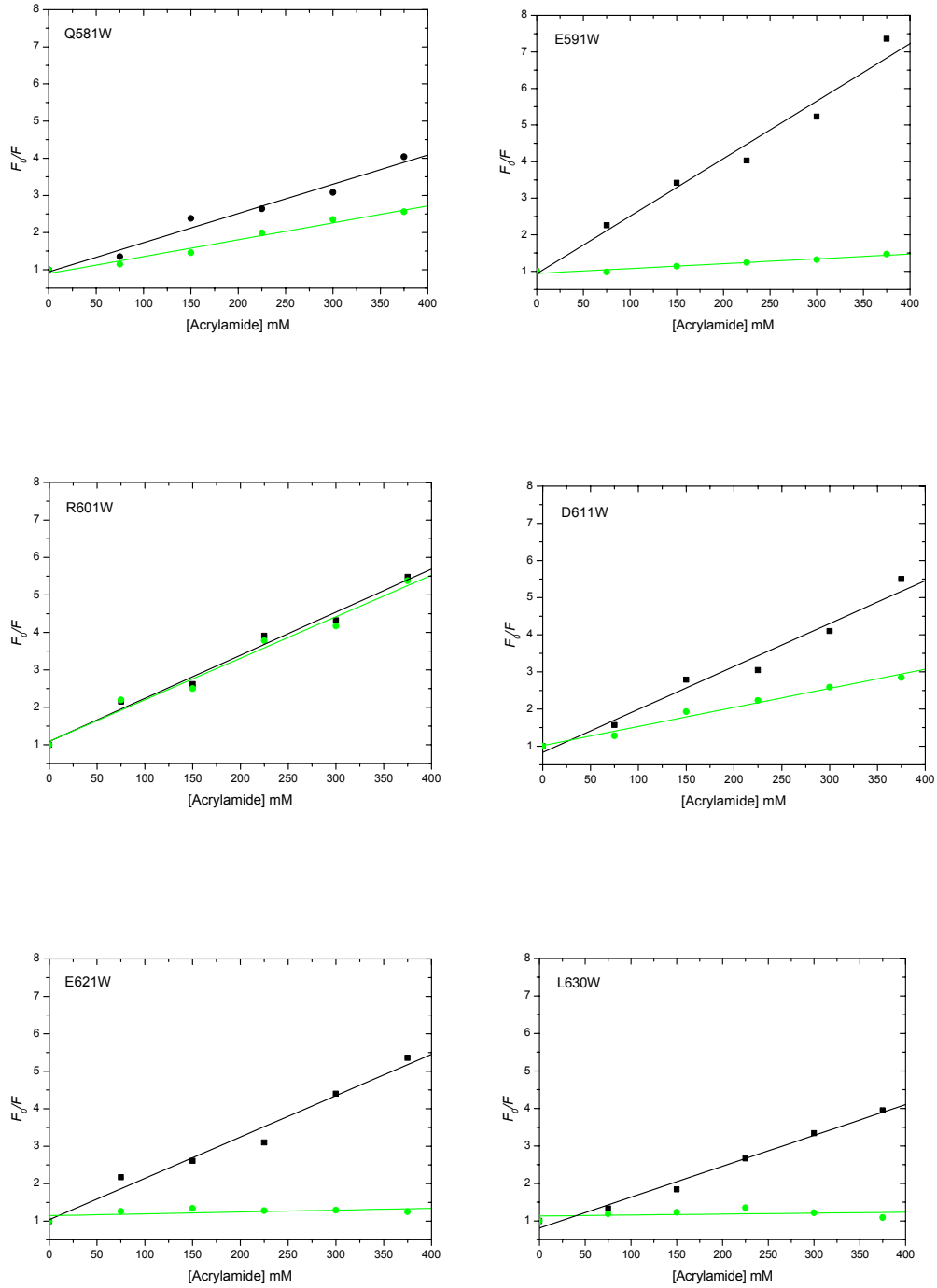

FIG 4.7.3. Stern-Volmer plots of Trp fluorescence quenching by acrylamide. Quenching experiments were conducted as described under "Experimental Procedures." In each panel the samples were investigated in the absence (■) and presence of (●) 150 μM PC/PG (60:40 % molar ratios). The slopes of the best fit lines for each data set (K_{SV} values) are shown in Table 4.7.3. Mean values ± standard deviation of two or three independent experiments are given.

Table 4.7.3. Stern-Volmer Constants of the Effect of PC:PG (60:40%) on Single-Trp Mutants of Loop 13 [a]
Fluorescence parameters were determined from the data shown in Figure 4.7.3.

Peptide	DOPC:DOPG (60:40 %) [b]	K_{SV} [c] (M^{-1})
Q581W	-	7.4
	+	4.5
E591W	-	15.2
	+	2.5
R601W	-	11.1
	+	10.6
D611W	-	8.8
	+	5.4
E621W	-	10.6
	+	1
L630W	-	8.4
	+	1

[a] Parameters of acrylamide accessibility were derived from the data shown in Figure 4.7.3.

[b] Quenching experiments were conducted in the absence (-) or presence (+) of 150 μM PC:PG (60:40%).

[c] The Stern-Volmer constants were determined from the slopes of the linear regression lines from plots of $F_0/F = 1 + K_{SV}[Q]$. Values are mean ± standard deviation of two or three independent experiments.

4.7.4. Effect of Lipid Composition on Trp Accessibility to Collisional Quenching

In addition, the calculated quenching constants of each Trp accessibility in the absence and presence of 150 μM pure PC and PC:PG (70:30 %) are shown in Table 4.7.4 (plots are not shown). The data shows that K_{SV} values for all mutants in the presence of pure PC and PC:PG (70:30%) are significantly lower as compared to the K_{SV} values in the presence of PC:PG (60:40%) vesicles. Thus, PC:PG (60:40%) vesicles are seem to favor the interaction and/or the orientation of loop 13 mutants more effectively with and/or within the membranes (see discussion).

Table 4.7.4. Influence of Lipid Composition of Vesicles on the Trp Fluorescence of Loop 13 Mutants.

Stern-Volmer constants (M^{-1}) for 3 μM of each Trp mutant in the absence and presence of vesicles (150 μM) of various compositions.

Parameters of [b] and [c] were derived from acrylamide quenching data (not shown).

Peptide	No lipid [a]	DOPC [b]	DOPC:DOPG (70:30 %) [c]
Q581W	7.4	6.6	n.d
E591W	15.2	11.8	7.3
R601W	11.1	13.4	11.4
D611W	8.8	8.2	6.1
E621W	10.6	11.0	1.5
L630W	8.4	7.8	1.9

[a,b,c] The Stern-Volmer constants were determined from the slopes of the linear regression lines from plots of $F_0/F = 1 + K_{SV}$ [Q] (Lackowicz, 1999). Values are mean ± standard deviation of two or three independent experiments.

n.d Not determined

5. DISCUSSION

5.1 Conformation of Loop 13

The elucidation of structure-function relationship of membrane peptides has been hindered by difficulties in expressing the complete peptide. We, therefore, chose to express a fragment of SGLT1 supposed to function in the receptor region for the inhibitor phlorizin. Six different single Trp mutants of loop 13 were over-expressed using site directed mutagenesis to investigate the binding of phlorizin in detail. The use of truncated loop 13 (amino acid residues 564-638) compared to the previously used complete loop 13 was favored in order to introduce reporter molecules at different positions of the loop, to increase the solubility and to avoid complications by intrapeptide disulfide bridge formation between cysteine 560 and 608 residue (Xia *et al*., 2003). The truncation of the molecule did, however, not interfere with the ability of the peptide to interact with phlorizin. The phlorizin dissociation constants in our studies are very similar to those determined for the formation of the initial collision complex by Oulianova and Berteloot's (1996) studies in intact membrane vesicles and also agree with the observed binding constant for complete loop 13 (Xia *et al*., 2003).

To facilitate the discussion of the secondary structure of loop 13, the predicted conformation based on the amino acid sequence is shown in Figure 5.1. In agreement with this prediction the maxima of Trp fluorescence of the various mutants differ. For example mutants 581 and 591 show a spectrum which has a maximum close to 350 nm, suggesting a random coil orientation of the neighbouring segments. For the other mutants e.g., 601, 611, 621 and 630, a more hydrophobic environment of the Trp can be assumed (blue shift of the maxima) suggesting a location in more ordered, probably α-helical structure (see Table 5.1). The presence of these α-helices in solution is confirmed by the CD spectrum that quite nicely reflects the relative abundance of the various conformations.

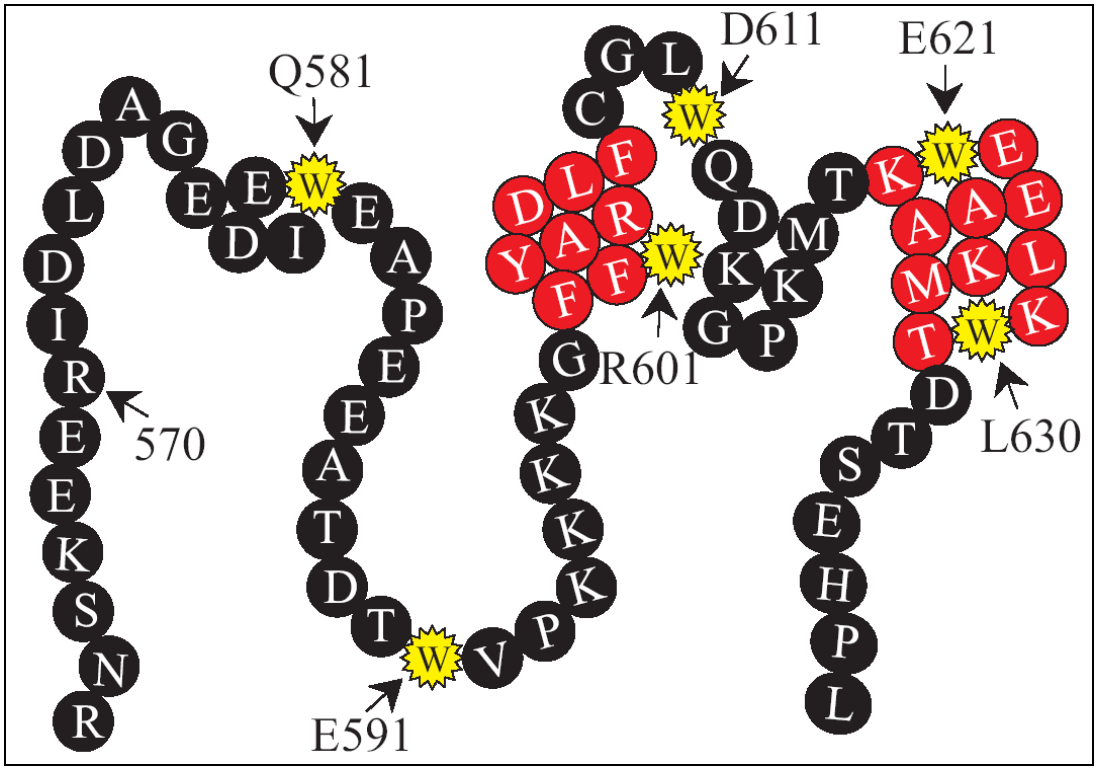

FIG. 5.1. A schematic two-dimensional model of loop 13 of SGLT1 (amino acid residues 564-638). *Yellow stars*, the positions of six single Trp mutations. *Red residues*, the predicted percentage of α-helices of domain. Only a single molecule with indicated positions of single Trp mutations is shown rather than six single-Trp mutants.

Table 5.1. Properties of Trp Mutants of Loop 13

Trp Mutants	Local environment of Trp in buffer	Positions of Trp residues in a peptide
Q581W	Hydrophilic	Random coil
E591W	Hydrophilic	Random coil
R601W	Hydrophobic	α-helix
D611W	Hydrophobic	Random coil (*located in between two α-helices*)
E621W	Hydrophobic	α-helix
L630W	Hydrophobic	α-helix

5.2 Interaction of Phlorizin with Loop 13

The strong sensitivity of Trp fluorescence intensity to peptide microenvironment is routinely exploited to follow a variety of protein conformational changes, e.g., ligand/substrate binding, folding/unfolding etc. (Callis and Vivian, 2003). The results of the studies with phlorizin are semi-quantitatively summarized in Table 5.2. Several major spectral changes are induced by phlorizin binding to loop 13. First, a red shift of the fluorescence maximum which indicates a transition between ordered (hydrophobic) to less ordered state of the loop (more hydrophilic). The most evident shift is observed for mutant D611W. Thus phlorizin binding appears to induce the opening of the region around amino acid 611 of loop 13, which before seems to be buried in between the two α-helices (see Figure 5.2 A).

The shift of the maximum of Trp fluorescence towards longer wavelength could, however, also be caused by a strong interaction of phlorizin associated water with the loop. Such a complex between phlorizin and water molecules can be formed by H-bonding between OH groups of phlorizin (e.g., mainly by 4-OH and 6-OH group of ring A and 4-OH of ring B). This would suggest a position of D611 in the binding pocket. A critical role of this region of loop 13 in phlorizin binding has also been proposed from studies on the intact carrier using site directed mutagenesis (Novakova *et al*., 2001) and from the biophysical studies using isolated loop 13 in solution (Xia *et al*., 2003, Xia *et al*., 2004).

The similar red shift in the fluorescence maximum of L630W is difficult to explain by the above assumption. Perhaps, in this part of loop 13, bound water molecules situated around the peptide contribute mostly to the signal. In other studies ligand induced conformational changes were also deduced from the fluorescence spectra. In this instance both water around the ligand and water around the peptide contributed to the shift, the contribution of each, in most cases, is difficult to estimate (Vivian and Callis, 2001).

Furthermore, fluorescence quenching was observed. We would like to correlate the quenching with the proximity of the indol ring of Trp to the phlorizin molecule. The main mechanism responsible for fluorescence quenching is charge/ energy transfer between phlorizin and Trp residues. Similar effects were observed for collagen fluorescence in the presence of varying concentrations of hypericin (Yova *et*

al., 2002; Yova *et al*., 1999). The maximum fluorescence quenching at the 611 position could then indicate that the phlorizin ring A is very close to the free indol ring of tryptophan. For the amino acids located in region 606-609 an interaction, although with slightly less affinity, would ensue. Thereby the binding site is defined. The minimum quenching observed for mutant L630W would suggest a positional arrangement of this part of loop far from the binding region. In case of mutants Q581W and E591W, significant quenching signals in the presence of phlorizin (see Table 5.2) might be attributed to a conformational change which brings this part of loop 13 somehow close to the binding site (see Figure 5.2 B).

Table 5.2. Effect of Phlorizin on Trp Fluorescence Parameters of Loop 13 Mutants

Trp Mutants	Red shift of fluorescence maximum	Quenching	Acrylamide accessibility
Q581W	+	++	-
E591W	++	++	++
R601W	+++	+++	+++
D611W	++++	++++	++++
E621W	+++	+++	+++
L630W	+++	+	-

+ correlates to high values
- correlates to low or non-significant values

A surprising result of this study is that the region especially between 591-621 is more accessible to acrylamide in the presence of phlorizin than in its absence (see Table 5.2). In our previous studies on phlorizin binding to loop 13 a protection effect of phlorizin was observed leading to a decreased accessibility of Trp at position 561 and its resonance partner Tyr at position 604 (Xia *et al*., 2003). The difference might be due to the fact, that in the former studies the peptide contained a disulfide bond which can alter the conformational changes significantly. The high accessibility of D611W towards acrylamide after phlorizin binding suggests that the interaction with phlorizin occurs in an aqueous environment; hence no protection effect is observed.

It is interesting to note that phloretin, the aglucone of phlorizin, induced qualitatively similar changes in D611W as phlorizin, although the effects on fluorescence and acrylamide accessibility were smaller. These results suggest that phloretin might bind to the same site as phlorizin. The larger disturbance of the conformation of loop 13 by phlorizin might be explained by the bulky nature of the glucose residue attached to the two aromatic rings. If phloretin indeed binds to the same site as phlorizin the non-competitive nature of the inhibition of D-glucose transport by phloretin might be due to a close coupling between loop 13 and the sugar translocating positions of SGLT1. Such coupling can occur by the formation of disulfide bonds between the extramembranous loops, direct evidence for the presence of such bonds has been obtained in our previous studies (Xia *et al*., unpublished results). In addition, we have also found ligand-induced conformational changes of SGLT1 in intact rabbit renal medullary brush-border membrane vesicles by monitoring the accessibility of extramembraneous cysteine residues with polyethylene oxide-maleimide activated biotin, followed by specific immunodetection of the biotin-coupled peptide (Xiaobing and Kinne-unpublished data) and by determining binding probability and unbinding force using antibodies against loop 13 attached to an atomic force microscopic cantilever (Wielert-Badt *et al*., 2002).

The conformation of phlorizin in aqueous solutions was previously studied by two-dimensional NMR and pharmacophore analysis by Wielert-Badt *et al*., 2000. Their model indicates that the interactions via hydrogen bonds from the 2-, 3-, 4-, and 6-hydroxyl groups (OH) of the pyranoside and the 4- and 6-OH of the aromatic ring A are essential for phlorizin binding. This information can now be combined with the Trp fluorescence data to estimate the dimensions of the phlorizin recognition and binding region. We can assume that the phlorizin binds to the region very close to position 611 by H-bonding probably with the 4-OH group by acceptor/donor atom O4 of the aromatic ring A. Thus, position 611 is supposed to be very important in phlorizin recognition as also suggested by the lower affinity of the D611W mutant. The H-bonding of any one hydrophobic amino acid residue located in 606-609 region with the 6-OH group by acceptor/donor atom O6 of the aromatic ring A of phlorizin also causes a strong interaction.

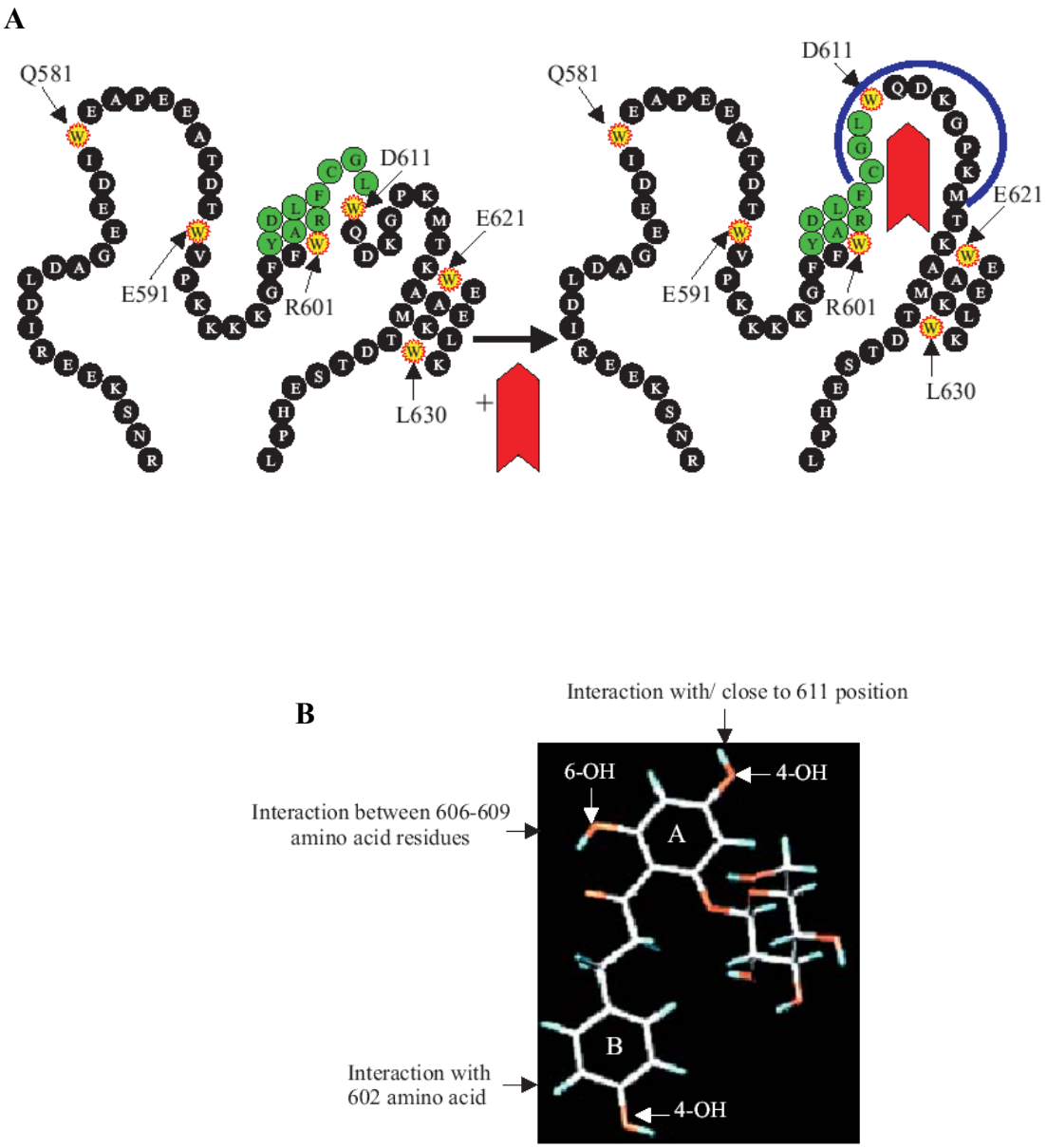

FIG. 5.2. A, Schematic two-dimensional model of loop 13 of rabbit SGLT1 (amino acids 564-638). *Left panel*: Arrangement of amino acids in the absence of phlorizin. α-helical areas are based on computer program and hydrophobicity of the Trp environment, arrangement of random coil takes into account the hydrophilicity of the Trp environment as predicted from the fluorescence maxima. *Right panel*: *yellow* stars represent the Trp mutations, *green* represents the presumed phlorizin-binding region; the *red arrow* indicates the proposed position of phlorizin in the binding region and the *blue arc* highlights the main area of conformational changes. The exposure of the region around position 611 to a more hydrophilic environment is derived from the strong red shift of the Trp fluorescence maximum. **B, three-dimensional conformation of phlorizin according to NMR studies by Wielert-Badt *et al*., 2000.** The arrows show the interactions of the aromatic ring A and B with the binding region (Raja *et al*., 2003).

On the basis of fluorescence studies of loop 13 in the presence of phlorizin, we could provide a generalized mechanism by which phlorizin inhibits sugar transport by SGLT1. According to our assumption, a phlorizin binding region in SGLT1 is located in between amino acids 601-611, in this region aromatic rings (A and B) of phlorizin interact with hydrophobic amino acids and the glucoside moiety of phlorizin is free to interact with sugar interaction sites of SGLT1 (Loo and Silverman, 1998; Diez-Sampedro *et al*., 2001). Previous mutagenesis studies provided evidence that also Asp-176 might be involved in determining the overall affinity of phlorizin to the transporter (Panayotova *et al*., 1994). Thus, there seems to be a close vicinity between loop 13 and Asp-176, again probably caused by disulfide bonds between various parts of the transporter.

According to our modeling assumptions based on secondary structure prediction and CD analysis, the regions especially between 599-607 and 620-631 around the binding pocket are in α-helical conformation. In the absence of phlorizin the region around amino acid 611 appears to interact with a part of the α-helical region, in particular with the hydrophobic amino acid residues between 606-609. Upon phlorizin binding this region becomes exposed to aqueous environment as shown by direction of the big red arrow in Figure 5.2 A.

In addition, the 4-OH group of the aromatic ring A comes close to position 611 effecting the Trp emission strongly (see Figure 5.2 B). At the same time the aromatic ring B comes conformationally close to position 600. Such a position has been identified in photoaffinity labeling studies with 3-azidophlorizin (Raja *et al*., 2003). We also propose that phlorizin binding results in reduction of van der Waals forces between parts of the two helices (e.g., interaction between 599-607 and 620-629 α-helical residues) while some parts of the α-helix (e.g., that close to position 630) are accessible to acrylamide irrespective of the presence of phlorizin.

It is necessary to discriminate the differences between an intact SGLT1 and isolated domain to understand the mechanism of interaction of various transport inhibitors *in vivo* as well as *in vitro*. Mutagenesis studies performed on intact SGLT1 showed that hydrophobic region (amino acid residues 604-610), located extracellulary in loop 13 are responsible for the interaction of phlorizin. In addition, the amino acids containing negative side chains affected the affinity of phlorizin drastically (Novakova *et al*., 2001). The experiments performed by over-expressing C-terminal

domain *in vitro* nicely reflected the changes in affinity of phlorizin to loop 13, as does the intact carrier. The specific method employed to observe conformational changes in an isolated loop 13 in the presence of phlorizin and the affinity of this domain are the major findings of the study presented here which could not be possible by using whole SGLT1.

All peptides need a specific three-dimensional structure to perform their particular function. Keeping in mind the difficulties in resolving the structure of mammalian membrane peptides, in general, and in the case of SGLT1 in particular, the use of SGLT1 fragments appears to be advantageous to study their function in more detail by using different biophysical methods, although the refinement of the assumed conformation and dimensions of phlorizin binding sites during SGLT1-inhibitor complex formation by NMR or x-ray crystallography is still required.

5.3. Interaction of Alkyl Glucosides with Loop 13

We observed basically three different parameters for the Trp fluorescence when n-hexyl-*β*-D-glucoside interacted with loop 13: (I) spectral shift in the fluorescence maximum, (II) fluorescence quenching, and (III) acrylamide accessibility. The changes observed are summarized semi quantitatively in Table 5.3. Since the affinity of *n*-hexyl-*β*-D-glucoside for the different mutants of loop 13 is quite similar, the differences in parameters I and III are interpreted as an indication of different conformational changes in different portions of loop 13. The quenching we notice in this study is probably due to positioning of the Trp molecule in the proximity of methionine, tyrosine, threonine, arginine, and/or lysine (Zhao and Kinnunen, 2002; Breukink *et al*., 1998) since the ligand *n*-hexyl-*β*-D-glucoside is spectroscopically silent. The protection against acrylamide is interpreted as a reduced accessibility of Trp caused by the fact that either the alkyl glucosides or a part of the loop shields Trp against the collision with acrylamide.

Table 5.3. Effect of n-Hexyl-β-D-glucoside on Trp Fluorescence Parameters of Loop 13 Mutants

Trp Mutants	Quenching	Spectral shifts	Acrylamide accessibility
Q581W	+	No change	-
E591W	No change	No change	-
R601W	+++	**Blue shift**	**- - - - (Strong decrease)**
D611W	++++	**Blue shift**	**- - (Decrease)**
E621W	+++++	**Red shift**	**+ (Increase)**
L630W	+++	**Strong blue shift**	**- - (Decrease)**

+ correlates to high values
- correlates to low values

The changes in the fluorescence of the various regions can be explained by the following events. For Q581W and E591W mutants, we did not observe significant changes suggesting that these positions do not participate in the interaction between

loop 13 and *n*-hexyl-*β*-D-glucoside (see Table 5.3). In a way, this is to be expected since computer modeling suggests a random orientation of this part of loop 13 (Raja *et al*., 2003 or under section 5.1).

The changes discussed below are compiled in the schematic model presented in Figure 5.3. For R601W, we observe a small blue shift in the maximum, a minor quenching, but maximum protection against acrylamide. The protection is probably caused by a strong binding of part of the alkyl glucoside in this area as also found in the photoaffinity labeling experiments where a direct interaction of the C2 position of the alkyl side chain with amino acids 598-601 could be demonstrated. The slight blue shift i.e., increase in hydrophilicity of the environment supports the assumption that the alkyl side chain is the part of the glucoside, which is binding. The experiments with 1-hexanol, where identical changes in the fluorescence of R601W were observed for 1-hexanol and *n*-hexyl-*β*-D-glucoside, point in the same direction.

The major change found for D611W is a strong quenching of fluorescence upon interaction with *n*-hexyl-*β*-D-glucoside. These data indicate that this area of loop 13 changes its position significantly with regard to neighboring areas of loop 13 but maintains its accessibility to acrylamide. The nearest neighbours responsible for major quenching could be the arginines at positions 601 and 602 or a methionine at position 618. Such a movement would require a high flexibility of this part of the molecule which is actually predicted by modeling, since this region is located in a random coil (Raja *et al*., 2003) between two helices (Raja *et al*., 2004, see also Figure 5.3).

E621W exhibits strong quenching and increased accessibility to acrylamide upon interaction with *n*-hexyl-*β*-D-glucoside. This probably also reflects the movement of the randomly coiled part of loop 13, although the specific interactions cannot be delineated currently with the data at hand. L630W exhibits the most prominent blue shift in the fluorescence maximum and a strong quenching by *n*-hexyl-*β*-D-glucoside. Thus, major changes occur in this region of loop 13. A more condensed state of the molecule that positions Trp 630 close to the helical (hydrophobic) part between amino acids 599 and 607 could explain both effects.

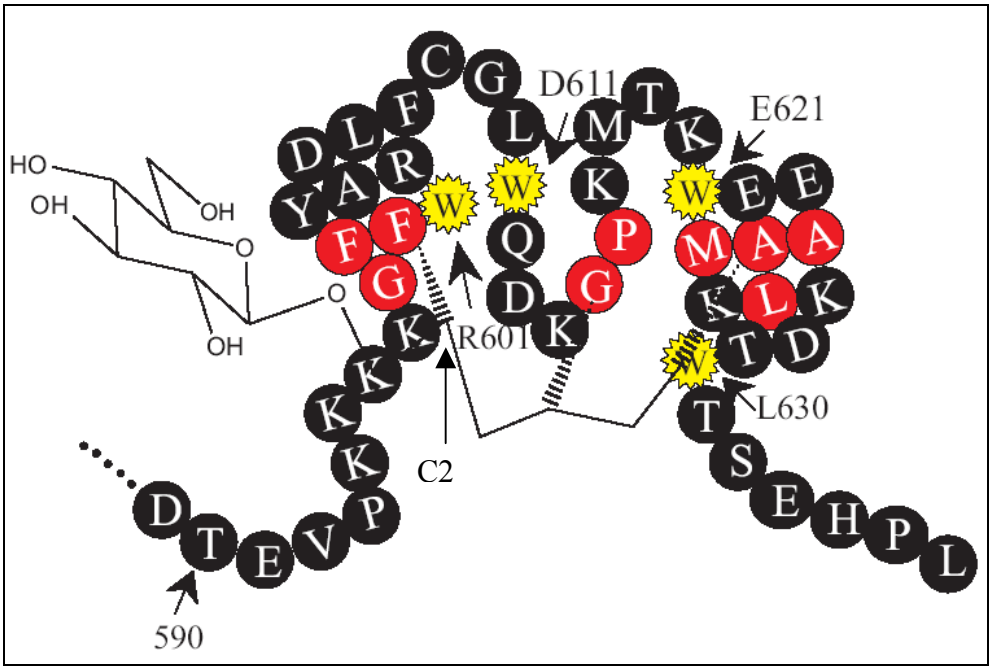

FIG. 5.3. Schematic two-dimensional model of *n*-hexyl-*β*-D-glucoside binding to the part of loop 13 of rabbit SGLT1. *Red residues* represent the assumed (hydrophobic sites of interaction between loop 13 and *n*-hexyl-*β*-D-glucoside. *Yellow stars* indicate single Trp mutations. C2 of the alkyl side chain is supposed to bind to the region between amino acids 598-601, C4 to 615-616 amino acid residues and C6 to the region between 621 to 630 amino acids. For further information see also previous studies (Raja *et al*., 2003 or under section 5.1).

The proposed model can be compared to the schematic two-dimensional model presented recently for the interaction between phlorizin and loop 13 (see under section 5.1). There, phlorizin unfolds the segment of loop 13 between amino acid residues 608 and 620; *n*-hexyl-*β*-D-glucoside on the other hand appears to condense loop 13 and buries this segment between the two putative small helices. This assumption is supported by the observation that in additional fluorescence quenching studies *n*-hexyl-*β*-D-glucoside prevents phlorizin from interacting with loop 13 (data not shown).

Thus, irrespective of the model assumed, it is clear that *n*-hexyl-*β*-D-glucoside interacts with loop 13. Interestingly, this interaction is quite strong, and the apparent affinities are close to those observed for the inhibition of D-glucose transport by the intact SGLT1 in natural membranes (Kipp *et al*., 1997). In addition, the relative potencies of the *α*- and *β*-glucosides and *cis* and *trans* derivatives of hexenyl glucosides on the transporter and in the isolated loop are comparable (Kipp *et al*., 1996). These results support the view that loop 13 contains structural elements that mimic the conditions prevailing in the intact SGLT1.

However, a word of caution is also necessary. There is a discrepancy between the results obtained for intact membrane-bound SGLT1 and study of an isolated loop13 with regard to the effect of chain length of alkyl glucosides on binding. In this study, strong binding was observed for a chain length of six to eight carbons, whereas inhibition of D-glucose transport was maximal with a chain length of 10 carbons in the alkyl side chain (Kipp *et al*., 1996). This observation might suggest that in the intact SGLT1 other parts of the transporter also interact with alkyl glucosides. However, it is also possible that the conformation of the peptides used here and that of loop 13 in the intact carrier is different. The truncation of loop 13 removes the cysteine at position 560 which can form a disulfide bridge and thus alter the conformation *in vivo*. One additional site of interaction, most probably for the glucose part of alkyl glucoside, is the sugar binding site of the transporter, which is similar to the observation with phlorizin (Frasch *et al*., 1970). This interaction predominates in the inhibition kinetics of the transport which is evident from the competition of D-glucose and *n*-hexyl-*β*-D-glucoside in the uptake studies.

5.4. Interaction of Loop 13 with Lipid Vesicles

For all mutants except 601, an increase in Trp fluorescence and blue shift in maximum was observed upon addition of negatively charged lipids which indicates the transfer of Trp residues from an aqueous to a hydrophobic environment (Breukink *et al*., 1998; Macek *et al*., 1995). The changes in the fluorescence observed for the various mutants after association with lipid vesicles are summarized in Table 5.4.

Table 5.4. Effect of Lipid Vesicles on Trp Fluorescence Parameters of Loop 13 Mutants

Peptide	Fluorescence	Blue shifts in maxima	Spin label proximity	Acrylamide accessibility	Positioning in bilayer
Q581W	**Increase**	**Very strong shift**	**Low**	**Decrease**	**Yes**
E591W	Increase	Slight shift	None	Maximum decrease	No
R601W	No change	No change	None	No change	No
D611W	Increase	Slight shift	Low	Decrease	No
E621W	**Increase**	**Strong shift**	**Present**	**Complete decrease**	**Yes**
L630W	**Max. Increase**	**Strong shift**	**Present**	**Complete decrease**	**Yes**

Interestingly these changes were not observed when pure PC vesicles were used. Since loop 13 contains several positively charged amino acids an interaction with the negatively charged head groups of PG is necessary for the association of the peptide to the lipids. The findings that in the presence of 30% PG less protection of each single Trp against acrylamide was observed than in the presence of 40% PG are consistent with this assumption.

As another major change, blue shifts in the maxima were observed. These indicate the positioning of the tryptophan into a more hydrophobic environment. In the experimental system employed here, this effect might be caused by insertion into the acyl side chains of the lipid phase of the phospholipids or due to a change in peptide conformation or both. We tested for the insertion into the lipid phase by employing doxyl labeled phospholipids and we now compare the two parameters.

For Q581W, we observed a very strong blue shift in the maximum and slight fluorescence quenching by doxyl groups. It thus can be assumed that this residue resides in the bilayer (see model in Figure 5.4). The significant protection against acrylamide in the presence of lipid vesicles also points in this direction. The discrepancy between the large change in the spectral maximum and the relative moderate effect of the doxyl quenchers can be explained by the fact that in the absence of the lipids Trp-581 resides in a very hydrophilic environment. The insertion into the hydrophobic lipids therefore causes the large blue shift.

E591W exhibits only a small blue shift, no quenching by doxyl derivations and maximum protection against acrylamide upon addition of lipid vesicles. Conformational changes of the peptide, such as positioning of one helix above the Trp-591 could result in a blue shift and maximum protection of this Trp against acrylamide.

Surprisingly, no significant change in parameters of Trp fluorescence was observed for R601W in the presence of vesicles, thus, this part of the peptide appears not be involved in interaction with the membrane. The positively charged poly lysine residues from position 594 to 597 strongly interact with the negatively charged polar head groups of the phospholipids, which form a major attachment site of the peptide. Studies performed by atomic force microscopy on lipid-peptide interaction suggest a similar situation (Wimmer *et al*., unpublished data; see also model in Figure 5.4).

For position 621 and 630 the strong blue shift in maxima and the quenching by doxyl labels strongly suggest immersion of this region into the acyl side chains of the phospholipids. The position of Trp-621 is probably closer to the center of the lipid bilayer than that of Trp-630 because the doxyl label at C5 and C12 quench the tryptophan fluorescence to the same extent in 621 where the effect of the label at C5 is stronger for Trp 630 (see model in Figure 5.4). This conclusion is also supported by the fact that both tryptophan residues become completely inaccessible to acrylamide and that this part of the peptide is also predicted to form a short hydrophobic α-helix. The reinsertion of the loop pulls 611 close to the membrane as evidenced by the decreased accessibility to acrylamide.

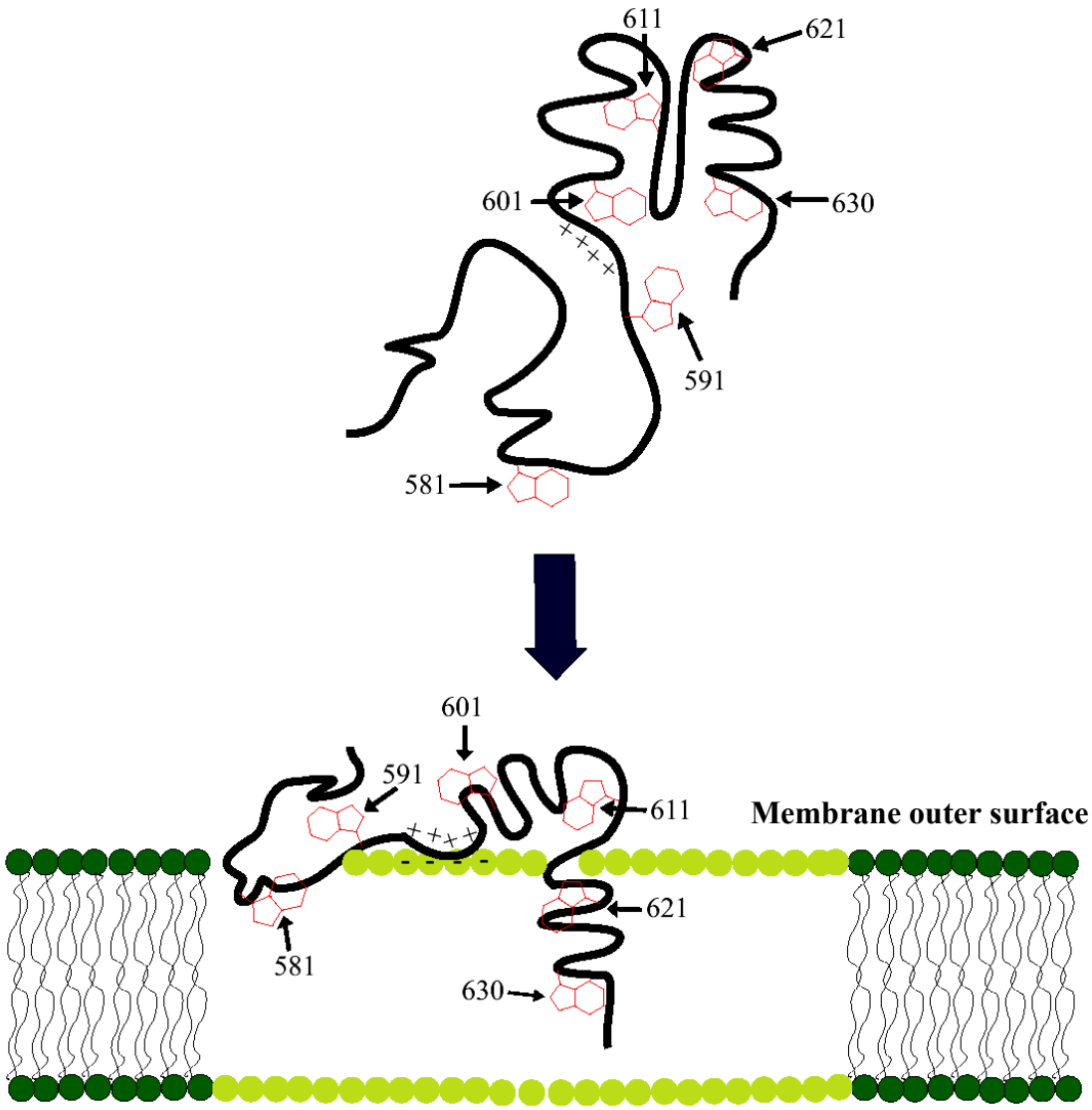

FIG. 5.4. Proposed two-dimensional model of the organization of Trp residues of Loop 13 in lipid vesicles. Trp residues at different positions are shown in red as aromatic rings with indol side chain. *Upper panel*: peptide conformation as depicted (Raja *et al*., 2003) in the absence of lipid vesicles, *Lower panel*: A conformation of the peptide assumed with Trp residues (*red*) in a lipid bilayer as suggested by the changes in Trp fluorescence parameters. Poly lysine region is also shown in a form of positive charges.

The topology of loop 13 in artificial membranes cannot assign the position of the early part of loop 13 studied here (amino acid residues 564-580) either inside or outside of the vesicles since no experimental data are available. The early parts of loop 13 also contain phosphorylation motifs for protein kinases at 562 position (Hediger *et al*., 1987) that in order to be physiologically relevant have to be exposed to the cytoplasm. A verification of an extramembranous orientation of late part of

loop 13 (amino acid residues 606-630) was studied by Wielert-Badt *et al*., 2002, by using molecular recognition atomic force microscopy on membrane vesicles. In addition to these studies, the findings are also consistent with the location of loop 13 which strongly reacts with an antibody, raised against amino acid residues 606-630, from outside of an intact SGLT1 (Lin *et al*., 1999).

In the present study, the topology of loop 13 in the membrane is consistent with the observations of *in vitro* as well as *in vivo* studies where phlorizin and alkyl glucosides interact with the hydrophobic parts of the transporter which were found on loop 13 (Novakova *et al*., 2001; Xia *et al*., 2003; Raja *et al*., 2003). The regions 600 to 611 as a phlorizin binding pocket and between 601 to 619 which contain binding sites for alkyl glucosides should be located extracellulary to provide interaction sites on SGLT1. Furthermore, the region 621 to 630 which is exposed to lipid bilayer phase in our fluorescence quenching studies contains another alkyl glucoside interaction region. Thus, the interaction of an alkyl side chain of an alkyl glucoside with the region in between 621 to 630 (predicted to be located in α-helical region) of loop 13 in a hydrophobic environment of lipid bilayer is most likely to be favored.

6. SUMMARY

SGLT1, a plasma membrane sodium/glucose cotransporter, is strongly inhibited by aromatic and aliphatic glucosides such as phlorizin and *n*-hexyl glucoside. We expressed a domain (loop 13), postulated to be involved in inhibitor binding, and labeled it with tryptophan reporter groups. Wild type and six mutants (Q581W, E591W, R601W, D611W, E621W and L630W) of loop 13 (amino acid residues 564-638) were expressed in *Escherichia coli* and purified to homogeneity. Changes in Trp quenching and positions of the emission maxima were determined in order to determine the conformational changes occurring during inhibitor binding.

After addition of phlorizin D611W displayed the largest quenching of 80%, followed by R601W (67%). It also exhibited the maximum red shift in Trp fluorescence (~14 nm), indicating an exposure of this region to a more hydrophilic environment. Titration experiments performed for each mutant showed a similar phlorizin affinity for all mutants. Also the maximum change in the collisional quenching constant by acrylamide was noted for D611W (K_{SV} = 11 M^{-1} in the absence of phlorizin and 55 M^{-1} in its presence). Similar results were obtained with phloretin. CD measurements and computer modeling revealed that D611W is positioned in a random coil situated between two α-helical segments. Taken together, these data indicate that phlorizin binding elicits changes in conformation leading to an 'opening' of loop 13. Modeling suggests an interaction of the 4- and 6-OH of the aromatic ring A of phlorizin with the region between amino acids 606 and 611. Phloretin seems to interact with the same region of the peptide. No quenching or protection was found for D-glucose.

Alkyl glucosides are also competitive inhibitors of the transport. Therefore, we searched for potential binding sites for alkyl glucosides in loop 13. To this end, we used a photoaffinity label (2′-Azi-*n*-octyl)-β-D-glucoside and analysed the region of attachment using MALDI-mass spectrometry producing wild type recombinant loop 13. Furthermore, experiments were conducted on single Trp mutants of loop 13 (Q581W, E591W, R601W, D611W, E621W and L630W) to determine the changes in fluorescence in the presence of alkyl glucosides, and accessibility of each Trp mutant to acrylamide. Photolabeling of loop 13 with (2′-Azi-*n*-octyl)-β-D-glucoside revealed

an attachment of the C2 group of the alkyl chain to Gly-Phe-Phe-Arg (amino acid residues 598-601). In the presence of *n*-hexyl-*β*-D-glucoside the mutants (R601W, D611W, E621W and L630W) showed a significant decrease in Trp fluorescence with an apparent binding affinity of 8-14 μM. Only L630W showed a significant blue shift and only in R601W was a change in acrylamide quenching (protection) observed. 1-hexanol produced the same results as *n*-hexyl-*β*-D-glucoside. The interaction shows stereo-selectivity for *n*-hexyl-*β*-D-glucoside binding; the *β*-configuration of the sugar moiety at C1, the *cis*-conformation of unsaturated alkenyl side chain at C3-C4, and the alkyl chain length of six to eight carbon atoms lead to an optimum interaction. A schematic two-dimensional model was derived in which C2 of the alkyl chain interacts with the region around residue 601, C3 and C4 interact with the region between residue 614 and 619, and C6-C8 interact with the region between residues 621 and 630.

The data demonstrate that loop 13 provides binding sites for alkyl glucosides as well as for phlorizin; but the regions of the peptide affected and the conformation assumed differ markedly. Thus, loop 13 of SGLT1 seems to be a major binding domain for the aglucone residues of competitive D-glucose transport inhibitors.

Furthermore, the interaction of loop 13 with lipid vesicles was monitored by reconstitution experiments of all Trp mutants of loop 13. An increase in Trp fluorescence, blue shifts in maxima and protection against acrylamide to a certain extent were observed for each mutant, except for R601W, which exhibited no change in these parameters. Mutants Q581W, E621W, and L630W exhibited a strong blue shift, suggesting their position in the lipid bilayer. By using membrane-embedded doxyl spin labels at 5- and 12-position of acyl side chain this position was confirmed by the quenching of these tryptophans. The protection of Q581W, E621W, and L630W against acrylamide supported the assumption that these parts of loop 13 are inserted into lipid vesicles. The other parts of the peptide appear to remain outside the lipid bilayer; the four lysine residues from position 594 to 597 forming an attachment site to negatively charged phospholipids. This attachment is a prerequisite for the insertion of parts of the peptide into the membranes since fluorescence changes were only observed in lipid vesicles containing phosphatidylglycerol (PG).

These studies thus reveal within one domain two different binding sites for inhibitors of the sodium-D-glucose cotransporter (SGLT1) which might act as targets

for the development of potential therapeutics to control sugar uptake in the intestine and kidney.

The topology studies confirm that the phlorizin binding domain between amino acid residues 601 to 611 and the alkyl glucoside binding domain between amino acid residues 601 to 619 reside outside the lipid bilayer and in vesicles is freely accessible to the inhibitor. For the alkyl glucosides additional interactions with the lipid bilayers appear to occur.

7. ABBREVIATIONS:

Arg	Arginine
BBMV	Brush border membrane vesicles
BisTris	2-[bis(2-hydroxyethyl)amino]-2-(hydroxymethyl)propane-1,3-diol
CD	Circular dichroism
cDNA	Complementary deoxyribonucleic acid
DNA	Deoxyribonucleic acid
dNTP	Deoxynucleotide triphosphate
Gln	Glutamine
Gly	Glycine
GST	Glutathione *S*-transferase
His	Histidine
K_d	Equilibrium dissociation constant
K_i	Inhibition constant
*K*m	Michaelis constant
K_{SV}	Collisional quenching constant
MALDI-TOF	Matrix-assisted laser desorption ionisation-time of flight
NMR	Nuclear Magnetic Resonance
PBS	Phosphate-buffered saline
Phe	Phenylalanine
rpm	Rotations per minute
SDS-PAGE	Sodium dodecylsulfate polyacrylamide gel electrophoresis
SGLT1	Na^+/D- glucose cotransporter
Thr	Threonine
Trp	Tryptophan
Tyr	Tyrosine
UV	Ultraviolet

8. REFERENCES

Beck, J.C., Sacktor, B. (1975) Energetics of the Na^+-dependent Transport of D-Glucose in Renal Brush Border Membrane Vesicles, *J. Biol. Chem.* **250:** 8674-8680

Breukink, E., Kraaij, C. V., Dalen, A. V., Demel, R. A., Siezen, R. J., Kruijff, B. D., and Kuipers, O. P. (1998) The Orientation of Nisin in Membranes, *Biochemistry* **37:** 8153-8162

Callis, P. V., and Vivian, J. T. (2003) Understanding the variable fluorescence quantum yield of tryptophan in proteins using QM-MM simulations. Quenching by charge transfer to the peptide backbone, *Chem. Phys. Lett.* **369:** 409-414

Diedrich, D. F. (1966) Competitive inhibition of intestinal glucose transport by phlorizin analogs*, Arch. Biochem. Biophys.* **117:** 248-256

Diez-Sampedro, A., Wright, E. M., and Hirayama, B. A. (2001) Residue 457 Controls Sugar Binding and Transport in the Na^+/Glucose Cotransporter, *J. Biol. Chem.* **276:** 49188-49194

Engelman, D.M., Steitz, T.A. (1981). The spontaneous insertion of proteins into and across membranes: the helical hairpin hypothesis, *Cell* **23:**411–422

Frasch, W., Frohnert, P. P., Bode, F., Baumann, K., and Kinne, R. (1970) Competitive inhibition of phlorizin binding by D-glucose and the influence of sodium: a study on isolated brush border membrane of rat kidney, *Pfluegers Arch.* **320:** 265-284

Fringes, M.A., Lin, J.T., Kinne, R.K.H. (2001) Functional Asymmetry of the Sodium-D-Glucose Cotransporter Expressed in Yeast Secretory Vesicles, *J. Membrane Biol.* **179:** 143-153

Gibbs, E.M., Hosang, M., Reber B.F.X., Semenza, G., and Diedrich, D. F. (1982) 4-Azidophlorizin, a high affinity probe and photoaffinity label for the glucose transporter in brush border membranes, *Biochim. Biophys. Acta.* **688:** 547-556

Hediger, M.A., Coady, M.J., Ikeda, T.S. and Wright, E.M. (1987) Expression cloning and cDNA sequencing of the Na^+/glucose cotransporter, *Nature* **330:** 379-381

Hirayama, B. A., Diez-Sampedro, A., and Wright, E. M. (2001) Common mechanisms of inhibition for the Na^+/glucose (hSGLT1) and Na^+/Cl^-/GABA (hGAT1) cotransporters, *Br. J. Pharmacol.* **134:** 484-495

Hirayama, B. A., Loo, D. D., and Wright, E. M. (1997) Cation Effects on Protein Conformation and Transport in the Na^+/Glucose Cotransporter, *J. Biol. Chem.* **272:** 2110-2115

Hunter, M.D. (1993) Variation in concentrations of phloridzin and phloretin in apple foliage, *Photochemistry (Oxford)* **34:** 1251-1254

Jacobs, R.E., White, S.H. (1989) The nature of the hydrophobic binding of small peptides at the bilayer interface: implications for the insertion of transbilayer helices, *Biochemistry* **28:**3421–3437

Kachalsky, S.G., Jensen, B.S., Barchan, D., and Fuchs, S. (1995) Two Subsites in the Binding Domain of the Acetylcholine Receptor: An Aromatic Subsite and a Proline Subsite, *PNAS* **92:** 10801-10805

Kipp, H., Kinne, R. K. H., and Lin, J. T. (1997) Synthesis of the photoaffinity label [1'-^{14}C]-6C-(azimethyl)octylglucoside and its reaction with isolated renal brush border membranes, *Anal. Biochem.* **245:** 61-68

Kipp, H., Kinne-Saffran, E. K., Bevan, C., and Kinne, R. K. H. (1997) Characteristics of renal Na^+-D-glucose cotransport in the skate (*Raja erinacea*) and shark (*Squalus acanthias*), *Am. J. Physiol.* **273:** R134-R142

Kipp, H., Lin, J. T., and Kinne, R. K. H. (1996) Interactions of alkyl glucosides with the renal sodium/D-glucose cotransporter, *Biochim. Biophys. Acta* **1282:** 124-130

Kyte, J., Doolittle, R.F. (1982) A simple method for displaying the hydropathic character of a protein, *J. Mol. Biol.* **157:**105–132

Lackowicz, J. R. (1999) *Principles of Fluorescence Spectroscopy*, Kluwer Academic/Plenum, New York

Lin, J. T., Hahn, K. D., and Kinne, R. K. (1982) Synthesis of phlorizin derivatives and their inhibitory effect on the renal sodium/D-glucose cotransport system, *Biochim. Biophys. Acta.* **693:** 379-388

Lin, J. T., Kormanec, J., Homerova, D., and Kinne, R. K. H. (1999) Probing Transmembrane Topology of the High-Affinity Sodium/Glucose Cotransporter (SGLT1) with Histidine-Tagged Mutants, *J. Membr. Biol.* **170:** 243-252

Lo, B., and Silverman, M. (1998) Cysteine Scanning Mutagenesis of the Segment between Putative Transmembrane Helices IV and V of the High Affinity Na^+/Glucose Cotransporter SGLT1, *J. Biol. Chem.* **273:** 29341-29351

Lockwood, N. A., Tu, R.S., Zhang, Z., Tirrell, M. V., Thomas, D. D. and Karim C. B. (2003) Structure and Function of Integral Membrane Protein Domains Resolved by Peptide-Amphiphiles: Application to Phospholamban, *Biopolymers* **69:** 283–292

Loo, D.D.F., Hirayama, B.A., Meinild, A.-K., Chandy, G., Zeuthen, Z. and Wright, E.M. (1999). Passive Water and Ion Transport by Cotransporters, *J. Physiol.* **518.1:**195-202

Lowry, O. H., Rosebrough, N. J., Farr, A. L., and Randall, R. J. (1951) Protein measurement with the folin phenol reagent, *J. Biol. Chem. 193*, 265-275

Macek, P., Zecchini, M., Pederzolli, C., Serra, M. D., and Menestrina, G. (1995) Intrinsic Tryptophan Fluorescence of Equinatoxin II, a Pore-Forming Polypeptide from the Sea Anemone *Actinia Equina* L, Monitors its Interaction with Lipid Membranes, *European Journal of Biochemistry* **234:** 329-335

McGuffin L. J., Bryson, K., and Jones D. T. (2000) The PSIPRED protein structure prediction server, *Bioinformatics*, **16:** 404-405

Meinild, A.-K., Klaerke, D. A., Loo, D. D. F., Wright, E. M., and Zeuthen, T.(1998) The human Na^+-glucose cotransporter is a molecular water pump, *The Journal of Physiology* **508.1:** 15-21

Michael, J.C., Jalal, F., Bissonnette, P., Cartier, M., Wallendorff, B., Lemay, G., Lapointe, J.Y. (2000) Functional Studies of a Chimeric Protein Containing

Portions of the Na^+ /Glucose and Na^+ /Myoinositol Cotransporters. *Biochim. Biophys. Acta* **1466:** 139-150

Murer, H., Hopfer, U., Kinne-Saffran, E., Kinne, R. (1974) Glucose Transport in Isolated Brush-Border and Lateral-Basal Plasma Membrane Vesicles from Intestinal Epithelial Cells, *Biochim. Biophys. Acta* **345:** 170-179

Neuhoff, V., Stamm, R., and Eibl, H. (1985) Clear background and highly sensitive protein staining with Coomassie Blue dyes in polyacrylamide gels: a systematic analysis, *Electrophoresis* **6:** 427-448

Novakova, R., Homerova, D., Kinne, R. K. H., Kinne-Saffran, E., and Lin, J. T. (2001) Identification of a region critically involved in the interaction of phlorizin with the rabbit sodium-D-glucose cotransporter SGLT1 *J. Membr. Biol.* **184:** 55-60

Oulianova, N., and Berteloot, A. (1996) Sugar transport heterogeneity in the kidney: two independent transporters or different transport modes through an oligomeric Protein? 1. Glucose transport studies, *J. Membr. Biol.* **153:** 181-194

Oulianova, N., Falk, S., and Berteloot, A. (2001) Two-step mechanism of phlorizin binding to the SGLT1 protein in the kidney, *J. Membr. Biol.* **179:** 223-242

Panayotova, H. M., Eskandari, S., Turk, E., Zampighi, G. A., and Wright, E. M. (1997) Five Transmembrane Helices Form the Sugar Pathway through the Na^+/Glucose Cotransporter, *J. Biol. Chem.* **272:** 20324-20327

Panayotova-Heiermann, M., Loo, D. D. F., Lostao, M. P., and Wright, E. M. (1994) Sodium D-Glucose Cotransporter Charge Movements
Involve Polar Residues, *J. Biol. Chem.* **269:** 21016-21020

Raja, M. M., Tyagi, N. K., and Kinne, R. K. H. (2003) Phlorizin Recognition in a C-terminal Fragment of SGLT1 Studied by Tryptophan Scanning and Affinity Labeling, *J. Biol. Chem.* **278:** 49154-49163

Raja, M. M., Kipp, H., and Kinne, R. K. H. (2004) C-Terminus Loop 13 of Na^+ Glucose Cotransporter SGLT1 Contains a Binding Site for Alkyl Glucosides, *Biochemistry* **43:** 10944-10951

Selinksky, B. S. (2003) Membrane Protein Protocols, Humana Press, Totowa, New Jersy, USA, page 497

Sierra, I. M. L. de la, Gallay, J., Vincent, M., Bertrand, T., Briozzo, P., Bârzu, O., and Gilles, A.-M. (2000) Substrate-Induced Fit of the ATP Binding Site of Cytidine Monophosphate Kinase from *Escherichia coli*: Time-Resolved Fluorescence of 3'-Anthraniloyl-2'-deoxy-ADP and Molecular Modeling, *Biochemistry* **39:** 15870-15878

Turk, E., Kerner, C.J., Lostao, M.P., Wright, E.M. (1996) Membrane topology of the human Na+/glucose cotransporter SGLT1, *J. Biol. Chem.* **271:** 1925–1934

Turk, E., Martý´n, M.G., Wright, E. (1994) Structure of the human Na+/glucose cotransporter gene *SGLT1, J. Biol. Chem.* **269:** 15204–15209

Turk, E., Wright, E.M. (1997) Membrane Topological Motifs in the SGLT Cotransporter Family, *J. Membrane Biol*. **159:** 1-20

Vayro, S., Lo, B., and Silverman, M. (1998) Functional studies of the rabbit intestinal Na+/glucose carrier (SGLT1) expressed in COS-7 cells: evaluation of the mutant A166C indicates this region is important for Na^+-activation of the carrier, *Biochem. J.* **332:** 119-125

Veenstra, M., Turk, E., Wright, E.M. (2002) A Ligand-dependent Conformational Change of the Na^+ /Galactose Cotransporter of Vibrio parahaemolyticus, Monitored by Tryptophan Fluorescence, *J. Membrane Biol.* **185:** 249-255

Vingron, M., Argos, P. (1988) A fast and sensitive multiple sequence alignment algorithm, *Computer Appl. Biosci.* **5:**115–121

Vivian, J. T., and Callis, P. V. (2001) Mechanisms of Tryptophan Fluorescence Shifts in Proteins, *Biophysical Journal* **80:** 2093-2109

von Heijne, G. (1992) Membrane protein structure prediction. Hydrophobicity analysis and the positive-inside rule, *J. Mol. Biol.* **225:**487–494

Wielert-Badt, S., Hinterdorfer, P., Gruber, H. J., Lin, J. T., Badt, D., Wimmer, B., Schindler, H., and Kinne, R. K. H. (2002) Single Molecule Recognition of Protein

Binding Epitopes in Brush Border Membranes by Force Microscopy, *Biophys. J.* **82:** 2767-2774

Wielert-Badt, S., Lin, J. T., Lorenz, M., Fritz, S., and Kinne, R. K. (2000) Probing the conformation of the sugar transport inhibitor phlorizin by 2D-NMR, molecular dynamics studies, and pharmacophore analysis, *J. Med. Chem.* **43:** 1692-1698

Wright, E. M. (1993) The intestinal Na^+/glucose cotransporter, *Annu. Rev. Physiol.* **55:** 575-589

Wright, E.M. (2001) Molecular Aspects of Intestinal Brush-Border Na^+ /glucose Transport, *Curr. Topics Membr.* **50:** 499-515

Wright, E.M. Loo, D.D.F., Panayotova-Heiermann, M., Hirayama, B.A. Turk, E., Eskandari, S., Lam, J.T. (1998) Structure and Function of the Na^+ /glucose Cotransporter, *Acta Physiol. Scand.* **163:** 257-264

Xia, X., Lin, C. T., Wang, G., and Fang, W. (2004) Binding of phlorizin to the C-terminal loop 13 of the Na^+/glucose cotransporter does not depend on the [560-608] disulfide bond, *Arch. Biochem. Biophys.* **425:** 58-64

Xia, X., Lin, J. T., and Kinne, R. K. H. (2003) Binding of Phlorizin to the Isolated C-Terminal Extramembranous Loop of the Na^+/Glucose Cotransporter Assessed by Intrinsic Tryptophan Fluorescence, *Biochemistry* **42:** 6115-6120

Yova, D., Hovhannisyan, V., Theodossiou, T., and Gukassyan, V. (2002) UV 98 List of paper and posters, *http://www.photobiology.com/UVR 98*

Yova, D., Theodossiou, T., and Hovhannisyan, V. (1999) *Laser - Tissue Interaction and Tissue Optics, Proc. SPIE.* **3565:** 174-180

Zhao, H., and Kinnunen, K. J. (2002) Binding of the Antimicrobial Peptide Temporin L to Liposomes Assessed by Trp Fluorescence, *J. Biol. Chem.* **277:** 25170-25177